IEEE Access
Multidisciplinary ⋮ Rapid Review ⋮ Open Access Journal

Received 20 July 2024, accepted 14 September 2024, date of publication 19 September 2024, date of current version 30 September 2024.

Digital Object Identifier 10.1109/ACCESS.2024.3464088

RESEARCH ARTICLE

Applications of Artificial Intelligence and PMU Data: A Robust Framework for Precision Fault Location in Transmission Lines

V. YUVARAJU[1], (Graduate Student Member, IEEE), S. THANGAVEL[1], (Senior Member, IEEE), AND MALLIKARJUNA GOLLA[2]

[1]Department of Electrical and Electronics Engineering, National Institute of Technology Puducherry, Karaikal 609609, India
[2]School of Electrical Engineering, Vellore Institute of Technology, Vellore, Tamil Nadu 632014, India

Corresponding author: Mallikarjuna Golla (mallikarjuna.golla@vit.ac.in)

This work was supported by Vellore Institute of Technology, Vellore Campus, Tamil Nadu.

ABSTRACT Providing continuous electric power supply to consumers is difficult for power system engineers due to various faults in transmission and distribution systems. Precise fault location (FL) in transmission lines speeds up the repair and restoration process. This paper proposes a wide neural network (WNN) approach for FL identification in power transmission networks. The proposed WNN uses the voltage, current magnitude, and phase angles measured by the phasor measurement unit (PMU). This proposed work considers the Western System Coordinating Council (WSCC) 9-bus test system with optimal PMU placement for fault analysis. The several types of faults created on different line sections of the test system are simulated using MATLAB/Simulink environment considering various fault parameters such as fault resistance, fault inception angle, and fault distance. The performance of the proposed scheme is measured by finding the absolute prediction error between actual and predicted FL. The results show that the average prediction errors for L-G, LL, LL-G, and LLL faults are 0.0121, 0.0209, 0.0139, and 0.0124, respectively. The proposed method outperforms the related machine learning-based FL estimation schemes for all the test cases considered at different fault locations. In addition, considering phase angle measurement improves the accuracy of finding the fault location compared to the voltage magnitude and current magnitude feature set.

INDEX TERMS Artificial intelligence, machine learning, phasor measurement unit, wide neural network, fault localization.

I. INTRODUCTION

The rapid increase in the energy demand necessitates expanding the power system, which increases the complexity [1]. Electrical power transmission and distribution systems are always vulnerable to the unexpected events which affect the system's steady-state performance [2]. Owing to the greater length of the transmission line (TL) , there are several possibilities for the occurrence of faults due to various causes such as equipment failures, creature activities, and natural phenomena [3]. In recent years, various blackouts have been recorded due to various types of faults and relay malfunctions in the power system network [4], [5]. This necessitates effective monitoring of the power system to ensure its reliability and security. TL faults are classified into series faults and shunt faults or short circuit faults. The occurrence of series faults is sporadic, and they can also be identified by observing the phase voltage [6]. There are two types of short circuit faults: symmetrical and unsymmetrical. Triple line (LLL) and triple line-to-ground (LLL-G) faults are symmetrical faults. Line-to-ground (L-G), line-to-line (LL), and double line-to-ground (LL-G) faults are examples of unsymmetrical faults. Symmetrical faults on transmission lines are rare, but their severity is high. Unsymmetrical faults are common, and they cause significant disruptions in the power system [6].

The associate editor coordinating the review of this manuscript and approving it for publication was Wei Wang.

All the aforementioned faults reduce the lifetime of the line components, increase the power loss, induce the heating effect on cables, and damage the insulators [7]. In addition, the short circuit faults in the power system severely affect its performance and create interruptions or disturbances in the energy supply and hence the reliability gets reduced [3]. Thus, the short-circuit faults are considered as severe faults in the transmission system. The effect of various types of faults on the power system depends on the type of fault, fault location (FL) from the relay point, and the duration of the fault. Hence, to improve the reliability of the power system network, accurate fault localization is required to fix the fault in time [8]. Therefore, an efficient method is needed to localize the TL faults for healing, which, in turn, reduces the system recovery time and maintains the power system's reliability.

The early prediction of fault needs relevant, accurate data. In this regard, using phasor measurement units (PMUs) enables the access of synchronized data in the power system network [9] to achieve the aforementioned tasks rather than the data from conventional measurements. PMUs are widely used in smart grids (SG) for time-synchronized measurement of current, voltage, phase angle, frequency, and rate of change of frequency. Due to the high cost of PMUs, the total number of PMUs should be minimized and optimally placed in a power system to achieve complete system observability [10], [11]. PMU measurements are widely used in power systems for protection applications such as TL fault identification, localization, and backup protection [12], [13], [14] and also the measured PMU data at various terminals are made available as inputs to intelligent techniques for effective fault detection, classification, and localization [15]. Nowadays, researchers are focusing on efficient FL estimation schemes to mitigate the effects of various types of faults in power system and restore system operation.

The FL identification methods are divided into three groups such as traveling wave-based, impedance-based, and artificial intelligence (AI) based methods [16]. In traveling wave-based methods, the total time taken by the waves to travel between the bus terminal and fault point is calculated, and it is used to estimate the FL [17]. In this method, the decision-making process depends on analyzing the position-time characteristics and the motion of the considered signals [16]. The traveling wave-based FL method for the line-to-ground fault is proposed in [18], and the fault distance (FD) is calculated using the difference of the wave's speed. In this group of methods, capturing the transient waveform for FL requires high-speed data acquisition devices, sensors, fault transient detectors, and a global positioning system (GPS) [19]. In the traveling wave-based methods, if the FL is closer to the bus-bar, then the accuracy in identification of FL is lesser [20].

The impedance-based FL methods are more popular among electric power utilities than the traveling wave method due to their simplicity and economy. The basic principle of the impedance-based method is to locate faults using the impedance value as seen from the measurement node [19]. Various types of impedance-based FL estimation methods are explored in [21], and also different strategies are offered to enhance their performance with high accuracy. The impedance-based FL method in [22] utilized the electrical quantities measured at both ends of the bus terminals, and it uses the faulty line parameters for the FL estimation. In [23], the Thevenin equivalent impedance of the network is used to estimate the FL, and in [24], line topology and source impedance-based fault locator is discussed. However, these approaches are one-ended, by utilizing equivalent circuits and statistical theories, they can significantly reduce parameter dependence. Further, these methods are extended for multi-terminal and non-homogeneous TLs in [25], [26], [27]. In the aforementioned impedance-based methods, the steady-state values of voltage and current during the fault are obtained, and are used to calculate an apparent impedance that is directly associated with FD. The multi-estimation is the major drawback in impedance-based methods due to the presence of multiple probable faulty points at the same location [28].

Nowadays, machine learning (ML) algorithms play a vital role in FL estimation with the arrival of a wide area monitoring system (WAMS) and the availability of big data [29]. The combination of artificial neural networks (ANN) and wavelet-based technique is used in [30] to locate TL faults. This method achieves lesser error in the estimation of FL. The comprehensive comparative analysis of performance in detecting, classifying, and localizing transmission line faults is presented in [31]. The authors compare the performance metrics for L-G, LL, and LL-G faults across various techniques such as adaptive neuro-fuzzy inference system (ANFIS), ANN, Discrete wavelet transform-Adaptive neuro-fuzzy inference system (DWT-ANFIS), and self-organizing map (SOM). Recently, incorporating renewable energy sources and the nonlinear behavior of advanced power electronic equipment pose significant challenges to power quality (PQ). In this regard, AI has become essential in developing intelligent control methods for PQ devices. In [32], the authors proposed the firefly algorithm-trained ANN controller (FF-ANNC) to resolve the PQ issues and enhance their performance.

Further, the ML and deep learning (DL) applications are extended to hardware fault prediction such as Embryonic Hardware (EmHW) in biomedical system and hardware fault prediction in the transistor level [33], [34]. AI-based techniques are widely used to detect the faults in solar photovoltaic (SPV) arrays and improve fault detection accuracy using a novel technique discussed in [35] and [36]. In [37], a support vector machine (SVM) with wavelet transform is used for short-circuit FL estimation in TLs. The complexities involved in FL estimation, especially in large-scale multi-machine power systems, necessitate a novel

method in FL estimation. Digital twin technology (DTT) has recently emerged as a solution by developing real-time digital replicas of physical equipment, facilitating efficient monitoring and fault diagnosis in power systems and subsea production systems [38], [39], [40]. In [41], the authors explored the use of a deep graph neural network (DGNN) that integrates multi-scale attention and a multi-linear perceptron block for fault localization, detection, and classification in transmission systems. However, the study noted a lower accuracy in fault localization.

Most of the previous works in the literature review used voltage or current features for fault location estimation. The wide area protection system requires the PMU data consisting of both the magnitude and phase angle of the considered signal to monitor the power system network and, hence, ensure the reliability of the power system. In addition, incorporating ML concepts with PMU data can effectively identify the FL. Finally, with the availability of PMU data, the proposed work presents a novel wide neural network (WNN) regression model to estimate the TL FL. The main contribution towards this work is as follows:

- A WNN-based scheme is developed and proposed for transmission line fault localization.
- The several types of faults on different line sections of the Western System Coordinating Council (WSCC) 9-bus test system are simulated by using MATLAB/Simulink considering various fault parameters such as fault resistance (FR), fault inception angle (FIA), and FD.
- The voltage, and current phasors for various fault scenarios are captured by PMUs, which are strategically positioned on the test system through optimal PMU placement (OPP) technique.
- The required datasets are generated using simulation and are used to train and test the WNN-based fault locator model.
- The effectiveness of the suggested model is assessed by comparing it with other regression-based state-of-the-art algorithms like decision tree (DT), and SVM, ANFIS, DWT-ANFIS, and DGNN in terms of performance metrics such as mean absolute error (MAE), mean squared error (MSE), and root mean squared error (RMSE).

The rest of this article is organized as follows: Section II describes the benchmark system used in this work for dataset preparation and parameters considered for the same. Section III presents the architecture and estimation methods of the proposed FL scheme. Section IV discusses the results and comparative analysis with other regression-based ML algorithms, and section V concludes the paper.

II. DATASET PREPARATION

The dataset preparation process for the proposed WNN-based fault localization techniques is elaborated in the following subsections:

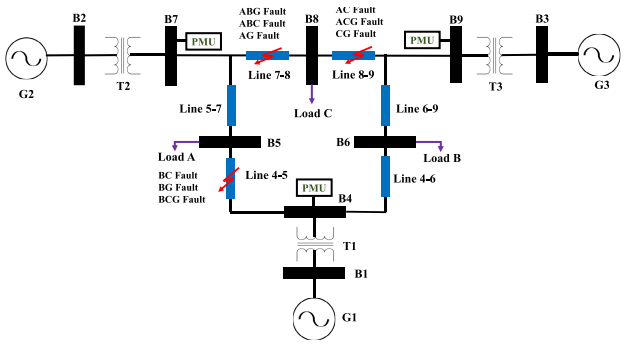

FIGURE 1. IEEE 9-bus test system with optimal PMU placement.

A. SYSTEM UNDER CONSIDERATION

The proposed fault localization scheme is tested on the WSCC 9-bus system [42]. It comprises three synchronous generators with a 60 Hz supply frequency, three two-winding transformers, six transmission lines, and three loads. The one-line diagram of the WSCC 9-bus system is shown in Figure 1.

B. OPTIMAL PMU PLACEMENT

The outlay of PMUs and their accessories motivate the researches on the OPP issues. OPP seeks to maximize the observability while utilizing the minimum number of PMUs. The teaching-learning-based optimization (TLBO) algorithm [43] is used to solve the OPP problem. Considering the characteristics of the TLBO algorithm, such as ease of implementation and non requirement of algorithm-specific parameters for tuning [43] inspires the researchers towards the TLBO algorithm in solving the OPP problem. The optimal number of PMUs reduces the cost and the optimal location yields the reliable operation. Hence, the authors in their previous article [11] proposed the TLBO-based algorithm for determining the optimal PMU locations. From this algorithm, the optimal PMU locations in a WSCC 9-bus system is found to be at bus-4, bus-7, and bus-9. Figure 1 shows the test system with optimally placed PMUs.

C. DATASET GENERATION

The performance of the WNN model in FL estimation of the WSCC 9-bus system is evaluated using Matrix laboratory (MATLAB)/Simulink environment for various types of faults on the TLs. Three-phase voltage and current signals with magnitude and phase angles are obtained from bus-4, bus-7, and bus-9 through PMUs placed at the aforementioned buses. The line-to-ground fault (C-G fault), line-to-line fault (AC fault), and double line-to-ground fault (AC-G fault) are created on TL 8-9 in the time interval of 200 ms to 300 ms. Two cycles of the post-fault voltage and current samples are considered within the specified time interval for dataset generation. The total number of samples considered for the two cycles is 68 (34 samples per cycle with a time step of 0.4902 ms and sampling frequency of 12 kHz). Table 1 shows

TABLE 1. Dataset generation parameters for line 8-9.

Parameters	Training Data	Test Data
Fault Type	C-G fault, AC fault, AC-G fault	C-G fault, AC fault, AC-G fault
Fault distance	1 km to 99 km with 1 km step size	C-G: 3.25 km to 95.25 km with 4 km step size AC: 1.75 km to 96.75 km with 5 km step size AC-G: 1.6 km to 96.6 km with 5 km step size
Fault resistance	30 Ω	300 Ω
Fault inception angle	0°	C-G : 0°, 15°, 45°, 75°, 105° AC : 0°, 60°, 90°, 120°, 180° AC-G : 0°, 10°, 30°, 40°, 50°
Total Number of Samples	99×1×1×68 = 6732 per fault	C-G : 24×1×1×68 = 1632 samples per FIA AC : 20×1×1×68 = 1360 samples per FIA AC-G : 20×1×1×68 = 1360 samples per FIA

TABLE 2. Dataset generation parameters for line 4-5.

Parameters	Training Data	Test Data
Fault Type	B-G fault, BC fault, BC-G fault	B-G fault, BC fault, BC-G fault
Fault distance	1 km to 99 km with 1 km step size	B-G: 1.6 km to 96.6 km with 5 km step size BC: 1.45 km to 96.45 km with 5 km step size BC-G: 4.75 km to 94.75 km with 5 km step size
Fault resistance	20 Ω	200 Ω
Fault inception angle	0°	B-G : 0°, 45°, 90°, 135°, 180° BC : 0°, 75°, 120°, 150°, 165° BC-G : 0°, 30°, 50°, 60°, 180°
Total Number of Samples	99×1×1×68 = 6732 per fault	B-G : 20×1×1×68 = 1360 samples per FIA BC : 20×1×1×68 = 1360 samples per FIA BC-G : 19×1×1×68 = 1292 samples per FIA

TABLE 3. Dataset generation parameters for line 7-8.

Parameters	Training Data	Test Data
Fault Type	A-G fault, AB fault, ABC fault, AB-G fault	A-G fault, AB fault, ABC fault, AB-G fault
Fault distance	1 km to 99 km with 1 km step size	A-G: 1.5 km to 96.5 km with 5 km step size AB: 3.25 km to 98.25 km with 5 km step size ABC: 4.75 km to 94.75 km with 5 km step size AB-G: 2.5 km to 98.5 km with of 4 km step size
Fault resistance	10 Ω	100 Ω
Fault inception angle	0°	A-G : 0°, 10°, 20°, 30°, 270° AB : 0°, 30°, 90°, 150°, 210° ABC : 0°, 30°, 40°, 50°, 150° AB-G: 0°, 10°, 30°, 50°, 180°
Total Number of Samples	99×1×1×68 = 6732 per fault	A-G: 20×1×1×68 = 1360 samples per FIA AB: 20×1×1×68 = 1360 samples per FIA ABC: 19×1×1×68 = 1292 samples per FIA AB-G: 25×1×1×68 = 1700 samples per FIA

the various fault parameters that are considered for dataset generation in lines 8-9.

For illustration, consider the C-G fault in lines 8-9. The fault is created at various locations from 1 to 99 km with a step size of 1 km, FR of 30 Ω, and FIA of 0°. So, the final dataset count for the C-G fault can be calculated as follows: (99×1×1×68) = 6732. Here, the "99" indicates the total number of fault locations for the C-G fault with a 1 km step size. The "1" in the second position indicates the number of FR (only one FR), and "1" in the third position indicates the number of FIA (only one FIA), and 68 indicates the total number of samples considered. Finally, the total number of datasets generated for the C-G fault is 6732. Similarly, the total number of training data samples was generated for the rest of the fault types, such as AC and AC-G faults in the same line sections 8-9. It is inferred from Table 1 that each type of fault has its own FL and FIA for testing data.

The total number of testing data samples is calculated based on the total number of fault distances for a particular fault type, FR, FIA, and the number of post-fault voltage and current cycles. The two cycles of post-fault voltage and current signals (with 68 samples) are also considered for

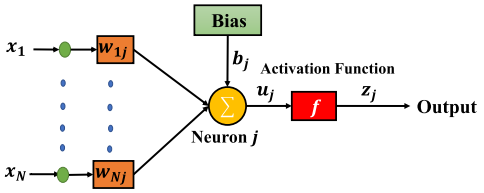

FIGURE 2. Structure of a typical neural network.

testing dataset generation. For example, the total number of dataset generation for the C-G fault (for testing) is demonstrated here. The C-G fault is created at various locations from 3.25 to 95.25 km with a step size of 4 km, FR of 300 Ω, and FIA of 0°. The total number of testing data samples generated for the C-G fault is calculated as follows: $24\times1\times1\times68 = 1632$ samples per FIA. Here, 24 indicates the total number of fault positions calculated based on the step size between 3.25 km to 95.25 km, "1" in position 2 indicates the total number of FRs, and "1" in position 3 denotes the total number of FIA. Here, the "68" indicates the total number of samples considered. Finally, the total number of testing datasets generated for the C-G fault is 1632 samples per FIA. Similarly, the testing dataset is generated for AC and AC-G faults for various test cases with different FIAs, which are shown in Table 1. Table 2 and Table 3 show the fault parameters for dataset generation for other types of faults on the TL 4-5 (B-G fault, BC fault, BC-G fault) and 7-8 (A-G fault, AB fault, ABC, and AB-G fault), respectively. The total number of data samples generated for training and testing is presented in Tables 2 and 3.

III. ARTIFICIAL NEURAL NETWORK

An ANN is an artificial system that mimics the operation of the brain in performing prediction (regression) and classification problems. It involves nodes, activation functions, weights, and biases that are linked in a network [44]. The neural network comprises an input layer representing the network's input data, hidden layers, and an output layer representing the network's response. Each layer has a certain number of neurons, and each neuron is linked to the neurons of the previous layer via adjustable weights w and biases b. Figure 2 shows the structure of a typical neural network unit. If $x_1, x_2, \cdots, x_N$ are the inputs of the j^{th} neuron then the output of the j^{th}*neuron* z_j is obtained as follows [45],

$$u_j = \sum_{i=1}^{N} w_{ij}x_i + b_j \tag{1}$$

$$z_j = f(u_j) \tag{2}$$

where w_{ij} represents the weight of the connection between the i^{th} input and neuron j, the bias of neuron j is represented by b_j, and the activation function of neuron j is represented by f.

The following features motivate the researchers toward ANN for transmission line FL identification.

- Due to simple and better generalization property, ability to learn independently and adaptive nature, ANN is widely used for fault analysis studies for both real-time and offline application [31].
- The ANN output is accurate, reliable and fast. Based on the training algorithm, the above-said task can be achieved [46].

A. PROPOSED FAULT LOCATOR SCHEME WITH TRAINING ALGORITHM

The proposed WNN architecture for FL estimation is shown in Figure 3. It has three layers: the input layer, a hidden layer, and an output layer. The data extracted from the MATLAB/Simulink model of the WSCC 9-bus system is used as the input and target data for training the WNN. For this, the network is initially trained with a set of training data consisting of post-fault voltage and current signals with magnitude and phase angles that are measured by PMUs located at optimal locations on the power system network. The proposed WNN architecture has one input layer that accepts 12 features, one hidden layer with 100 neurons, and an output layer for estimating the fault location. The inputs layers are used to transfer the inputs to hidden layers. Using the weight of the connection between the input and the hidden layer, the bias, and the activation function of the hidden layer, the output of the hidden layer is obtained. The output z_j of neuron j is obtained as follows:

$$z_j = f_{hidden}\left(\sum_{i=1}^{N} w_{ij}^{hidden}x_i + b_j^{hidden}\right) \tag{3}$$

where f_{hidden} is the activation function of the hidden layer, w_{ij}^{hidden} represents the weight of the connection between the i^{th} neuron of the input layer and neuron j in the hidden layer and b_j^{hidden} represents the bias of neuron j.

In modern WNN, the rectified linear unit (ReLU) activation function is widely used during the feed-forward training, which is defined as [47] and [48]

$$ReLU(x) = x^+ = max(0, x) \tag{4}$$

The vanishing-gradient problem is well handled by ReLU [47], [48], and it is less computationally expensive than traditional hyperbolic tangent and sigmoid activation operations [48]. As a result, ReLU is extremely useful when developing WNN and deep neural networks. The output vector y_1 of the output layer is calculated using the weight that connects the hidden and output layers, the bias of the output layer, and the activation function. The value of y_1 with one neuron is obtained as follows:

$$y_1 = f_{out}\left(\sum_{j=1}^{M} w_j^{out}z_j + b_{out}\right) \tag{5}$$

where f_{out} is the activation function of the output layer, w_j^{out} represents the weight of the connection between the j^{th} neuron of the hidden layer and the neuron in the output layer, b_{out} represents the bias of the output layer. The pure linear activation function is used in the output layer.

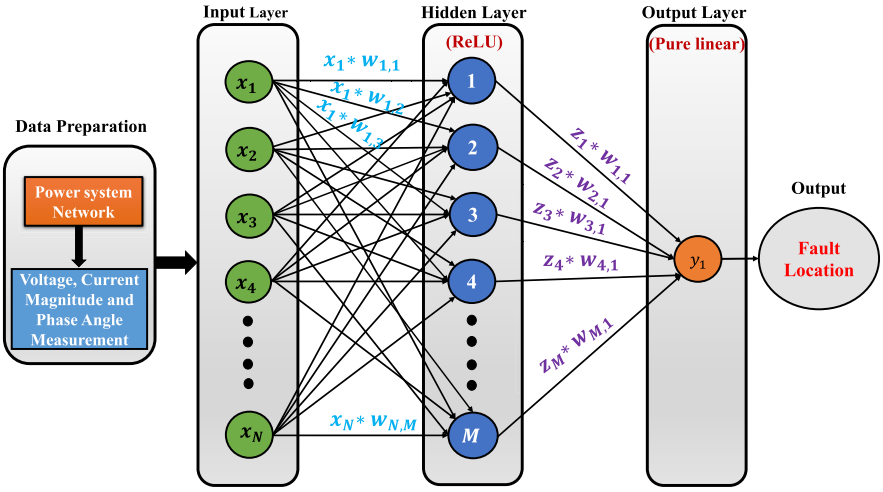

FIGURE 3. Architecture of the proposed wide neural network.

TABLE 4. Performance evaluation during C-G fault at line 8-9.

Metrics	Training Results			Testing Results														
				Test - I			Test - II			Test - III			Test - IV			Test - V		
	WNN	DT	SVM	WNN	DT	SVM	WNN	DT	SVM	WNN	DT	SVM	WNN	DT	SVM	WNN	DT	SVM
MAE	0.0037	0.0021	1.9363	0.0037	0.2702	1.8989	0.0055	0.2831	1.9214	0.0090	0.3223	1.9950	0.0102	0.3343	2.0274	0.0087	0.3184	1.9879
MSE	0.0000	0.0018	4.7736	0.0000	0.0831	4.6109	0.0000	0.0996	4.8167	0.0001	0.1557	5.4315	0.0002	0.1769	5.7004	0.0001	0.1487	5.3855
RMSE	0.0047	0.0423	2.1849	0.0048	0.2882	2.1473	0.0070	0.3156	2.1947	0.0111	0.3946	2.3306	0.0129	0.4205	2.3875	0.0112	0.3856	2.3207

TABLE 5. Performance evaluation during AC fault at line 8-9.

Metrics	Training Results			Testing Results														
				Test - I			Test - II			Test - III			Test - IV			Test - V		
	WNN	DT	SVM	WNN	DT	SVM	WNN	DT	SVM	WNN	DT	SVM	WNN	DT	SVM	WNN	DT	SVM
MAE	0.0063	0.0004	1.6474	0.0050	0.2510	1.6351	0.0059	0.2633	1.6993	0.0051	0.2548	1.6294	0.0054	0.2577	1.5638	0.0056	0.2673	1.6448
MSE	0.0001	0.0004	3.6772	0.0000	0.0636	3.6322	0.0001	0.0757	4.0371	0.0000	0.0677	3.5817	0.0000	0.0706	3.1677	0.0001	0.0809	3.6960
RMSE	0.0084	0.0211	1.9176	0.0066	0.2522	1.9061	0.0081	0.2752	2.0092	0.0067	0.2601	1.8925	0.0071	0.2657	1.7798	0.0078	0.2844	1.9225

TABLE 6. Performance evaluation during AC-G fault at line 8-9.

Metrics	Training Results			Testing Results														
				Test - I			Test - II			Test - III			Test - IV			Test - V		
	WNN	DT	SVM	WNN	DT	SVM	WNN	DT	SVM	WNN	DT	SVM	WNN	DT	SVM	WNN	DT	SVM
MAE	0.0059	0.0208	2.0079	0.0061	0.4343	2.0280	0.3598	0.4416	2.0246	0.3631	0.4818	2.0487	0.3852	0.4928	2.0796	0.4442	0.5046	2.1048
MSE	0.0001	0.0021	5.0471	0.0001	0.1943	5.1398	0.1768	0.2075	5.1188	0.1821	0.2882	5.3817	0.2146	0.3137	5.6445	0.2883	0.3740	5.8885
RMSE	0.0097	0.0456	2.0247	0.0098	0.4408	2.2671	0.4205	0.4552	2.2625	0.4267	0.5369	2.3198	0.4633	0.5601	2.3758	0.5369	0.6115	2.4266

TABLE 7. Performance evaluation during B-G fault at line 4-5.

Metrics	Training Results			Testing Results														
				Test - I			Test - II			Test - III			Test - IV			Test - V		
	WNN	DT	SVM	WNN	DT	SVM	WNN	DT	SVM	WNN	DT	SVM	WNN	DT	SVM	WNN	DT	SVM
MAE	0.0241	0.0028	1.4218	0.0242	0.4447	1.4149	0.0706	0.4283	1.3245	0.0398	0.4463	1.3561	0.0610	0.4472	1.3983	0.0443	0.4493	1.3502
MSE	0.0018	0.0027	2.8014	0.0018	0.2047	2.7434	0.0079	0.1891	2.2492	0.0049	0.2062	2.5426	0.0066	0.2071	2.8303	0.0059	0.2101	2.5262
RMSE	0.0426	0.0518	1.6737	0.0430	0.4524	1.6563	0.0887	0.4348	1.4997	0.0698	0.4541	1.5945	0.0813	0.4550	1.6824	0.0769	0.4584	1.5894

The output y_1 is predicted FL, represented as $y^{predicted}$. After obtaining the predicted FL, the performance and effectiveness of the proposed model are evaluated. In this regard, various performance metrics are used to validate the proposed model, such as MAE, MSE, and RMSE, which reflect the performance of the proposed WNN model. The

TABLE 8. Performance evaluation during BC fault at line 4-5.

Metrics	Training Results			Testing Results														
				Test - I			Test - II			Test - III			Test - IV			Test - V		
	WNN	DT	SVM	WNN	DT	SVM	WNN	DT	SVM	WNN	DT	SVM	WNN	DT	SVM	WNN	DT	SVM
MAE	0.0128	0.0200	1.7823	0.0139	0.4872	1.7592	0.2091	0.5025	1.9561	0.2530	0.5057	2.0239	0.1205	0.4972	1.7396	0.0954	0.4962	1.8122
MSE	0.0004	0.0228	4.0291	0.0005	0.2408	3.9585	0.0560	0.2584	5.4053	0.0815	0.2619	5.8589	0.0241	0.2523	3.8226	0.0146	0.2509	4.3631
RMSE	0.0204	0.1509	2.0007	0.0225	0.4907	1.9896	0.2366	0.5084	2.3249	0.2855	0.5117	2.4205	0.1555	0.5023	1.9552	0.1207	0.5009	2.0888

TABLE 9. Performance evaluation during BC-G fault at line 4-5.

Metrics	Training Results			Testing Results														
				Test - I			Test - II			Test - III			Test - IV			Test - V		
	WNN	DT	SVM	WNN	DT	SVM	WNN	DT	SVM	WNN	DT	SVM	WNN	DT	SVM	WNN	DT	SVM
MAE	0.0079	0.0010	1.6837	0.0068	0.2516	1.6514	0.0717	0.2539	1.7188	0.0742	0.2519	1.6583	0.0256	0.2825	1.8921	0.0258	0.2705	1.6692
MSE	0.0002	0.0010	3.7267	0.0001	0.0640	3.6031	0.0074	0.0664	4.0357	0.0098	0.0644	3.6506	0.0014	0.1130	3.7924	0.0014	0.0830	3.6947
RMSE	0.0126	0.0322	1.9305	0.0106	0.2531	1.8982	0.0861	0.2576	2.0089	0.0992	0.2538	1.9107	0.0378	0.3258	1.9882	0.0377	0.2881	1.9222

TABLE 10. Performance evaluation during A-G fault at line 7-8.

Metrics	Training Results			Testing Results														
				Test - I			Test - II			Test - III			Test - IV			Test - V		
	WNN	DT	SVM	WNN	DT	SVM	WNN	DT	SVM	WNN	DT	SVM	WNN	DT	SVM	WNN	DT	SVM
MAE	0.0104	0.0015	1.8558	0.0111	0.5000	1.8611	0.0103	0.5007	1.8606	0.0131	0.5015	1.8603	0.0174	0.5000	1.8632	0.0287	0.5647	1.9436
MSE	0.0003	0.0015	4.3743	0.0003	0.2500	4.3814	0.0004	0.2515	4.3735	0.0007	0.2529	4.3766	0.0011	0.2500	4.4013	0.0017	0.3956	5.2488
RMSE	0.0168	0.0385	2.0915	0.0185	0.5000	2.0932	0.0193	0.5015	2.0913	0.0259	0.5029	2.0920	0.0334	0.5000	2.0979	0.0418	0.6290	2.2910

TABLE 11. Performance evaluation during AB fault at line 7-8.

Metrics	Training Results			Testing Results														
				Test - I			Test - II			Test - III			Test - IV			Test - V		
	WNN	DT	SVM	WNN	DT	SVM	WNN	DT	SVM	WNN	DT	SVM	WNN	DT	SVM	WNN	DT	SVM
MAE	0.0223	0.0038	1.7580	0.0228	0.0038	1.7607	0.0390	0.3471	1.7144	0.0451	0.4148	1.6380	0.0320	0.3015	1.7689	0.0542	0.4067	1.7059
e MSE	0.0019	0.0034	4.3035	0.0019	0.0034	4.3221	0.0059	0.1824	3.9859	0.0064	0.3278	3.6377	0.0026	0.1140	4.4269	0.0097	0.2880	4.0395
RMSE	0.0436	0.0583	2.0745	0.0433	0.0583	2.0790	0.0770	0.4271	1.9935	0.0798	0.5725	1.9073	0.0507	0.3377	2.1040	0.0986	0.5367	2.0098

TABLE 12. Performance evaluation during ABC fault at line 7-8.

Metrics	Training Results			Testing Results														
				Test - I			Test - II			Test - III			Test - IV			Test - V		
	WNN	DT	SVM	WNN	DT	SVM	WNN	DT	SVM	WNN	DT	SVM	WNN	DT	SVM	WNN	DT	SVM
MAE	0.0096	0.0002	1.8783	0.0106	0.5467	1.7331	0.0257	0.5557	2.2224	0.1416	0.5623	2.5640	0.0839	0.5735	2.8567	0.0848	0.5495	1.8845
MSE	0.0003	0.0007	4.3632	0.0003	1.5695	3.8632	0.0222	1.6260	7.5259	0.0318	1.6209	10.0490	0.0113	1.6298	12.2920	0.0130	0.6043	4.9886
RMSE	0.0159	0.0129	2.0888	0.0182	1.2528	1.9655	0.0471	1.2751	2.7433	0.1783	1.2732	3.1700	0.1065	1.2767	3.5059	0.1138	1.2667	2.2335

TABLE 13. Performance evaluation during AB-G fault at line 7-8.

Metrics	Training Results			Testing Results														
				Test - I			Test - II			Test - III			Test - IV			Test - V		
	WNN	DT	SVM	WNN	DT	SVM	WNN	DT	SVM	WNN	DT	SVM	WNN	DT	SVM	WNN	DT	SVM
MAE	0.0318	0.0145	2.1618	0.0318	0.4979	2.1617	0.1377	0.4984	2.1723	0.0346	0.5099	2.2026	0.2456	0.5201	2.2586	0.0480	0.5010	2.1725
MSE	0.0022	0.0117	5.7304	0.0022	0.2479	5.7663	0.0280	0.2484	5.8253	0.0029	0.2716	6.1657	0.0909	0.2930	6.7132	0.0053	0.2541	5.8218
RMSE	0.0469	0.1080	2.3938	0.0472	0.4979	2.4013	0.1674	0.4984	2.4136	0.0541	0.5211	2.4831	0.3015	0.5413	2.5910	0.0729	0.5041	2.4128

aforementioned metrics denote the prediction error rate, and each one is defined as follows [49], [50]: MAE, commonly used for regression models, measures the average magnitude of the errors between actual and predicted FL values, calculated as follows:

$$MAE = \frac{1}{T}\sum_{k=1}^{T}|(y_k^{actual} - y_k^{predicted})| \tag{6}$$

MSE, another crucial metric, measures the average of the squared differences between actual and predicted FL values, and is expressed as follows:

$$MSE = \frac{1}{T}\sum_{k=1}^{T}(y_k^{actual} - y_k^{predicted})^2 \tag{7}$$

RMSE, a quadratic metric, is determined by taking the square root of the mean of the squared differences between the actual

TABLE 14. Actual and predicted fault location with error during C-G fault at line 8-9.

Actual Fault Location (km)	Predicted Fault Location (km) and Error for different Test cases									
	Test - I	Error	Test - II	Error	Test - III	Error	Test - IV	Error	Test - V	Error
3.25	3.2549	-0.0049	3.2485	0.0015	3.2632	-0.0132	3.2404	0.0096	3.2120	0.0380
7.25	7.2493	0.0007	7.2491	0.0009	7.2460	0.0040	7.2458	0.0042	7.2557	-0.0057
11.25	11.2418	0.0082	11.2494	0.0006	11.2424	0.0076	11.2309	0.0191	11.2275	0.0225
15.25	15.2548	-0.0048	15.2499	0.0001	15.2530	-0.0030	15.2416	0.0084	15.2391	0.0109
19.25	19.2548	-0.0048	19.2503	-0.0003	19.2517	-0.0017	19.2432	0.0068	19.2412	0.0088
23.25	23.2456	0.0044	23.2503	-0.0003	23.2441	0.0059	23.2393	0.0107	23.2370	0.0130
27.25	27.2492	0.0008	27.2503	-0.0003	27.2485	0.0015	27.2508	-0.0008	27.2519	-0.0019
31.25	31.2366	0.0134	31.2501	-0.0001	31.2313	0.0187	31.2240	0.0260	31.2215	0.0285
35.25	35.2528	-0.0028	35.2499	0.0001	35.2482	0.0018	35.2298	0.0202	35.2218	0.0282
39.25	39.2443	0.0057	39.2498	0.0002	39.2451	0.0049	39.2462	0.0038	39.2472	0.0028
43.25	43.2306	0.0194	43.2496	0.0004	43.2503	-0.0003	43.2755	-0.0255	43.2823	-0.0323
47.25	47.2585	-0.0085	47.2496	0.0004	47.2576	-0.0076	47.2704	-0.0204	47.2747	-0.0247
51.25	51.2487	0.0013	51.2497	0.0003	51.2387	0.0113	51.2489	0.0011	51.2398	0.0102
55.25	55.2556	-0.0056	55.2497	0.0003	55.2615	-0.0115	55.2801	-0.0301	55.2897	-0.0397
59.25	59.2610	-0.0110	59.2500	0.0000	59.2808	-0.0308	59.3097	-0.0597	59.3189	-0.0689
63.25	63.2472	0.0028	63.2503	-0.0003	63.2541	-0.0041	63.2745	-0.0245	63.2817	-0.0317
67.25	67.2503	-0.0003	67.2506	-0.0006	67.2567	-0.0067	67.2642	-0.0142	67.2658	-0.0158
71.25	71.2351	0.0149	71.2510	-0.0010	71.2348	0.0152	71.2372	0.0128	71.2387	0.0113
75.25	75.2623	-0.0123	75.2513	-0.0013	75.2591	-0.0091	75.2524	-0.0024	75.2511	-0.0011
79.25	79.2687	-0.0187	79.2515	-0.0015	79.2617	-0.0117	79.2500	0.0000	79.2461	0.0039
83.25	83.2525	-0.0025	83.2515	-0.0015	83.2507	-0.0007	83.2483	0.0017	83.2408	0.0092
87.25	87.2629	-0.0129	87.2512	-0.0012	87.2595	-0.0095	87.2515	-0.0015	87.2494	0.0006
91.25	91.2605	-0.0105	91.2505	-0.0005	91.2404	0.0096	91.2501	-0.0001	91.2449	0.0051
95.25	95.2634	-0.0134	95.2492	0.0008	95.2611	-0.0111	95.2585	-0.0085	95.2571	-0.0071

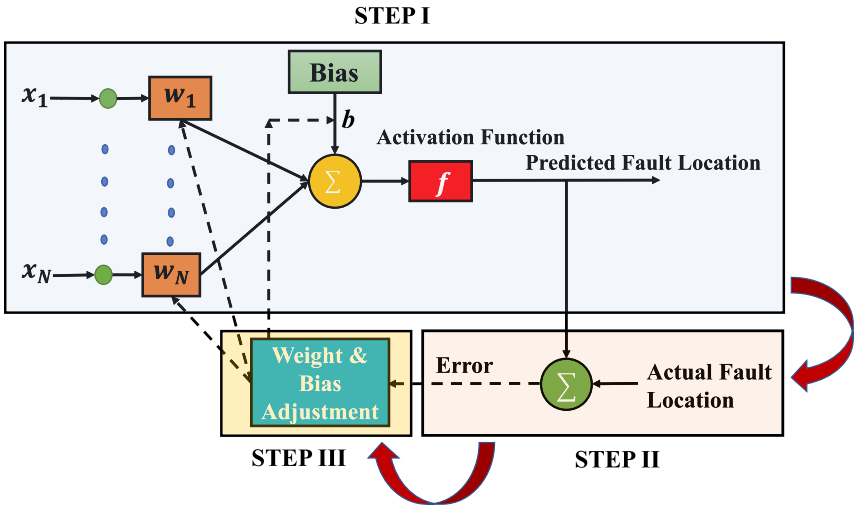

FIGURE 4. Step by step working of wide neural network.

and predicted FL values. The formula for RMSE is as follows:

$$RMSE = \sqrt{\frac{1}{T}\sum_{k=1}^{T}(y_k^{actual} - y_k^{predicted})^2} \quad (8)$$

where T is the number of input data, y^{actual} is the actual output and $y^{predicted}$ is the output of the WNN model. The training algorithm plays a vital role in tuning the connection weights w and biases b. The step-by-step process of the

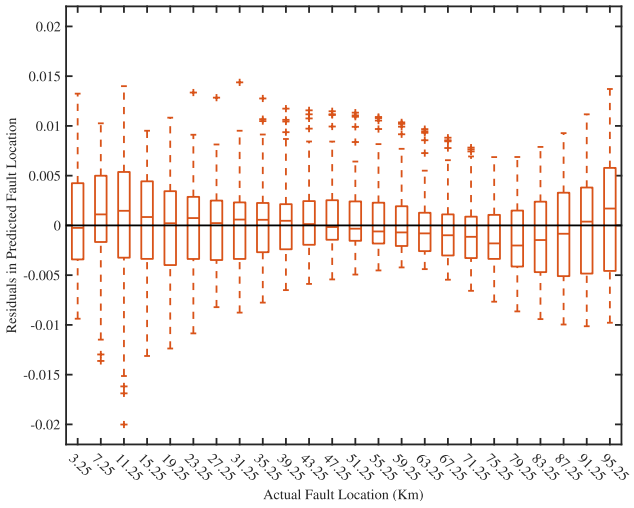

(a) Test case - I with 0° FIA

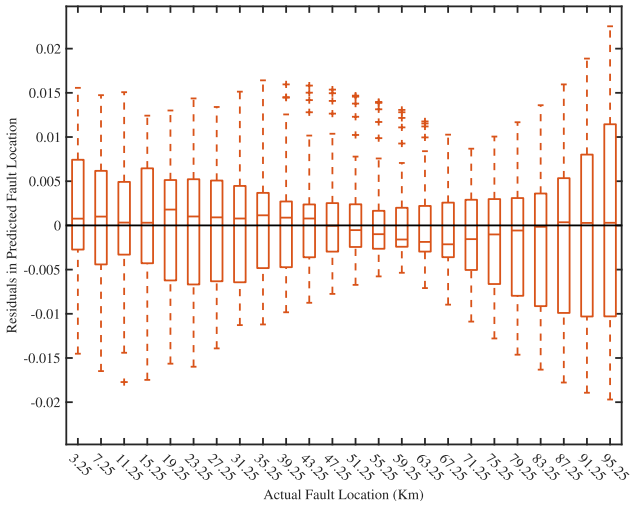

(b) Test case - II with 15° FIA

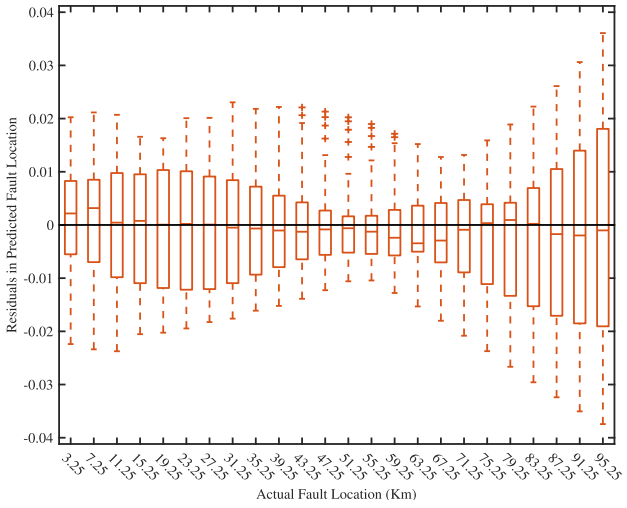

(c) Test case - III with 45° FIA

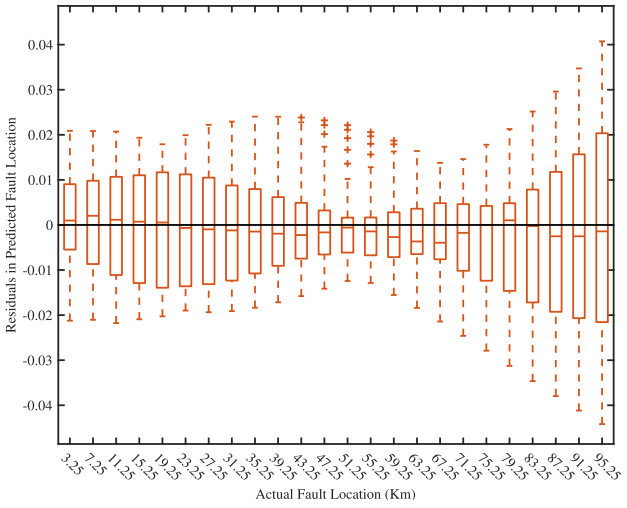

(d) Test case - IV with 75° FIA

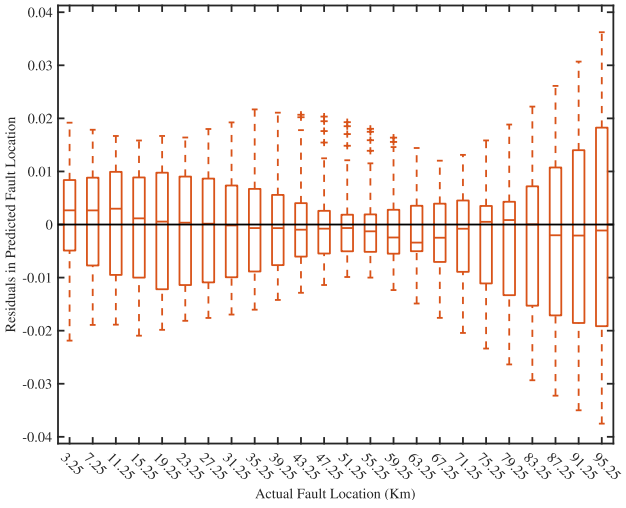

(e) Test case - V with 105° FIA

FIGURE 5. **Residuals in predicted fault location during C-G fault at line 8-9.**

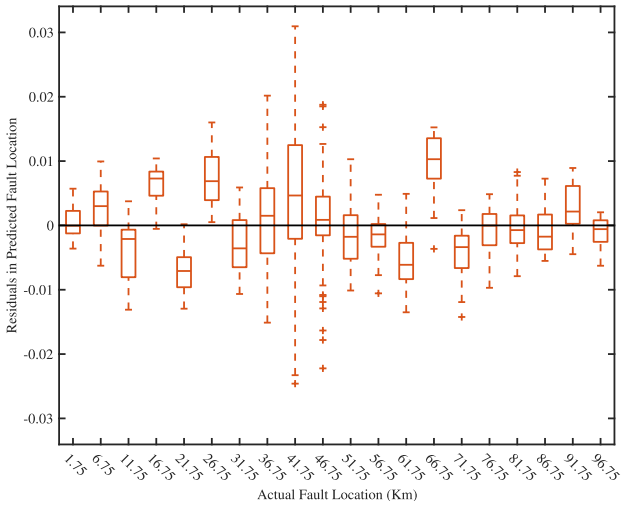

(a) Test case - I with 0° FIA

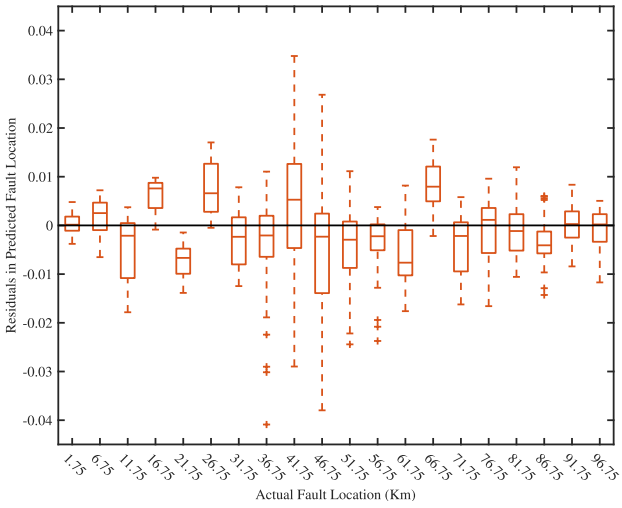

(b) Test case - II with 60° FIA

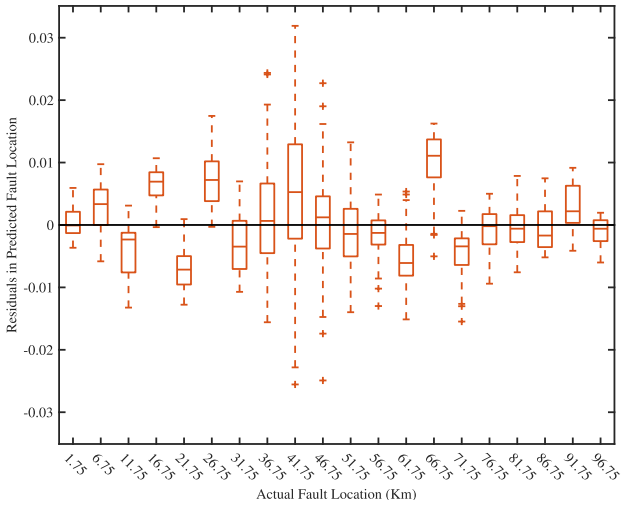

(c) Test case - III with 90° FIA

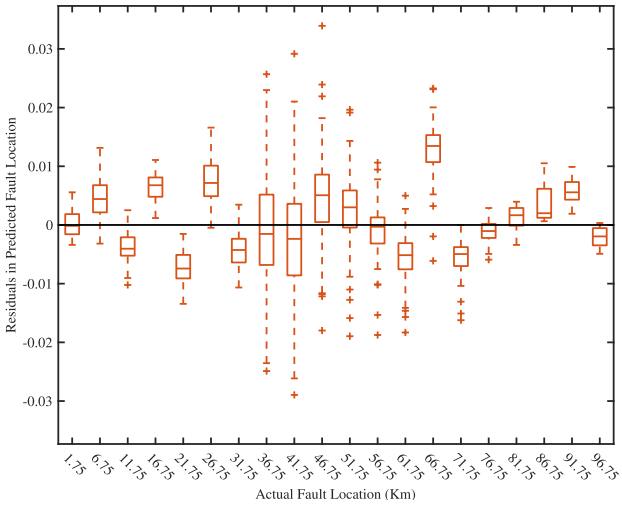

(d) Test case - IV with 120° FIA

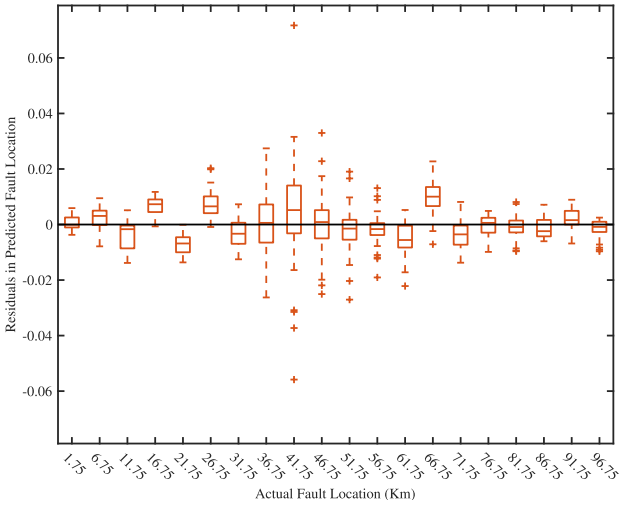

(e) Test case - V with 180° FIA

FIGURE 6. **Residuals in predicted fault location during AC fault at line 8-9.**

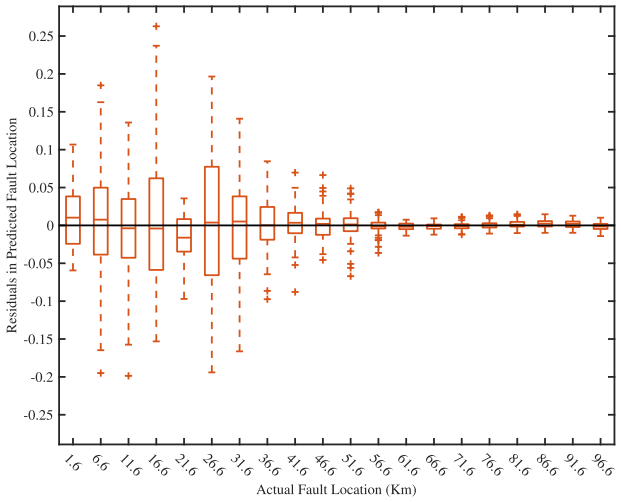

(a) Test case - I with 0° FIA

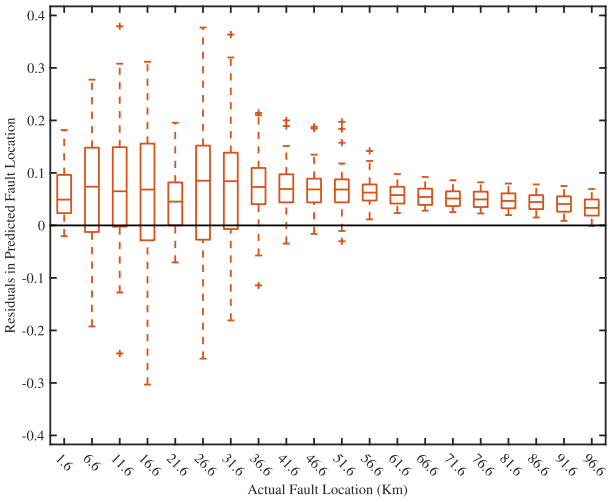

(b) Test case - II with 45° FIA

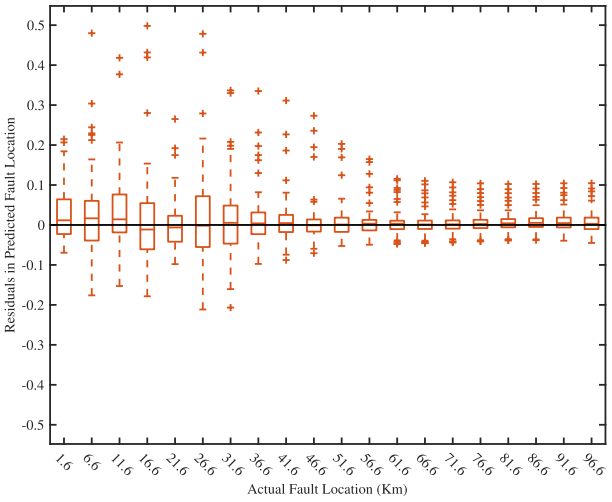

(c) Test case - III with 90° FIA

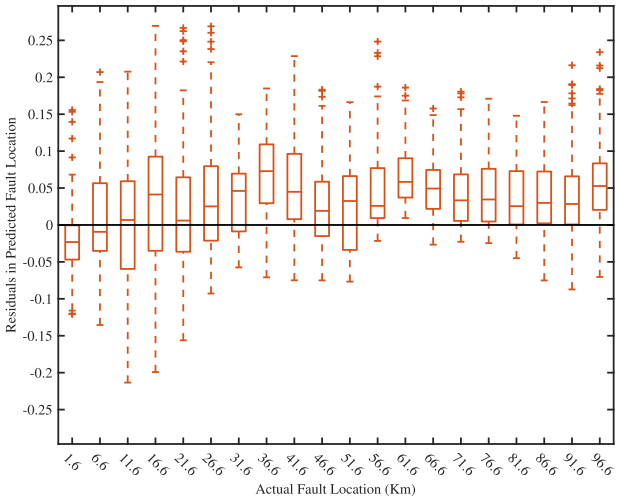

(d) Test case - IV with 135° FIA

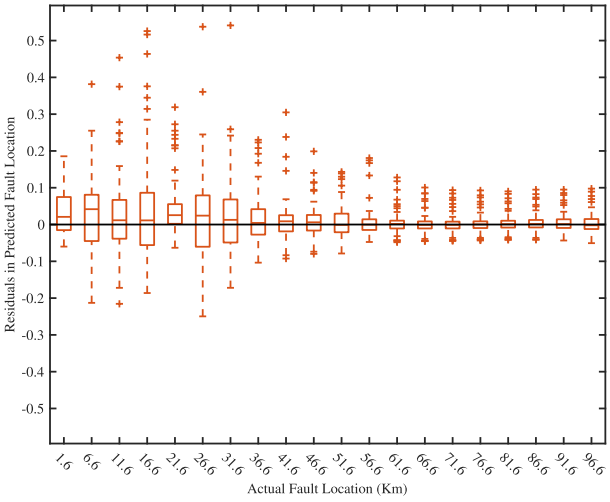

(e) Test case - V with 180° FIA

FIGURE 7. **Residuals in predicted fault location during B-G fault at line 4-5.**

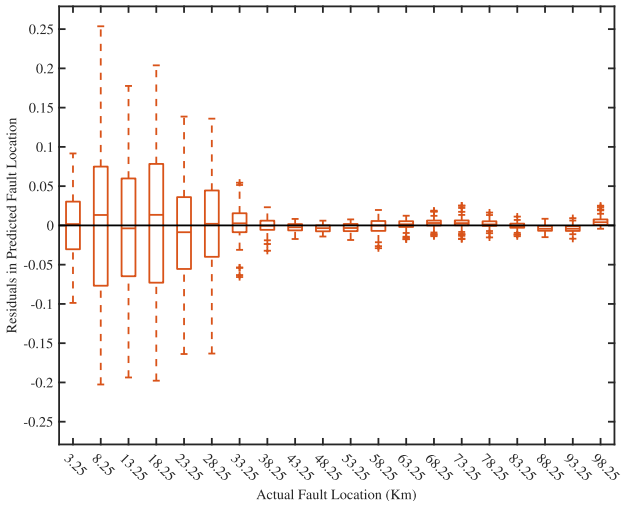

(a) Test case - I with 0° FIA

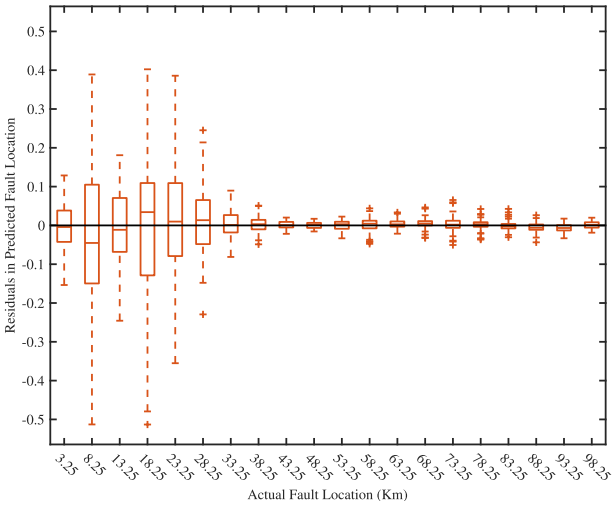

(b) Test case - I with 30° FIA

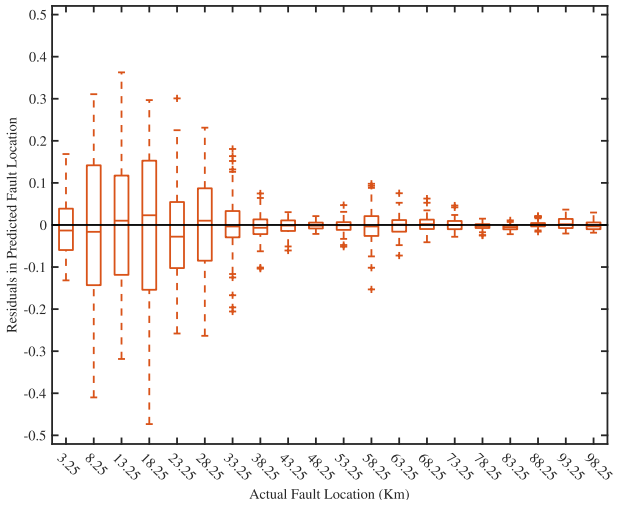

(c) Test case - III with 90° FIA

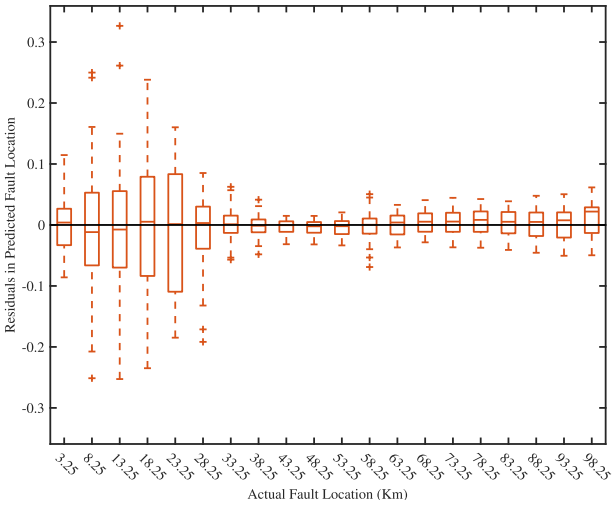

(d) Test case - IV with 150° FIA

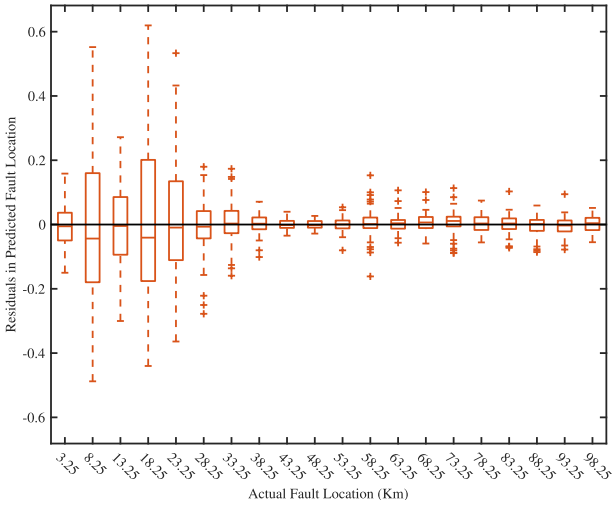

(e) Test case - V with 210° FIA

FIGURE 8. **Residuals in predicted fault location during AB fault at line 7-8.**

TABLE 15. Actual and predicted fault location with error during AC fault at line 8-9.

Actual Fault Location (km)	Predicted Fault Location (km) and Error for different Test cases									
	Test - I	Error	Test - II	Error	Test - III	Error	Test - IV	Error	Test - V	Error
1.75	1.7497	0.0003	1.7499	0.0001	1.7497	0.0003	1.7496	0.0004	1.7495	0.0005
6.75	6.7474	0.0026	6.7503	-0.0003	6.7482	0.0018	6.7470	0.0030	6.7453	0.0047
11.75	11.7540	-0.0040	11.7509	-0.0009	11.7548	-0.0048	11.7540	-0.0040	11.7538	-0.0038
16.75	16.7438	0.0062	16.7492	0.0008	16.7437	0.0063	16.7438	0.0062	16.7437	0.0063
21.75	21.7573	-0.0073	21.7512	-0.0012	21.7573	-0.0073	21.7572	-0.0072	21.7572	-0.0072
26.75	26.7427	0.0073	26.7487	0.0013	26.7425	0.0075	26.7427	0.0073	26.7425	0.0075
31.75	31.7529	-0.0029	31.7519	-0.0019	31.7526	-0.0026	31.7532	-0.0032	31.7542	-0.0042
36.75	36.7489	0.0011	36.7489	0.0011	36.7537	-0.0037	36.7484	0.0016	36.7508	-0.0008
41.75	41.7454	0.0046	41.7494	0.0006	41.7444	0.0056	41.7453	0.0047	41.7528	-0.0028
46.75	46.7494	0.0006	46.7503	-0.0003	46.7556	-0.0056	46.7494	0.0006	46.7458	0.0042
51.75	51.7517	-0.0017	51.7517	-0.0017	51.7542	-0.0042	51.7512	-0.0012	51.7477	0.0023
56.75	56.7517	-0.0017	56.7507	-0.0007	56.7533	-0.0033	56.7516	-0.0016	56.7509	-0.0009
61.75	61.7553	-0.0053	61.7543	-0.0043	61.7557	-0.0057	61.7553	-0.0053	61.7556	-0.0056
66.75	66.7403	0.0097	66.7483	0.0017	66.7418	0.0082	66.7401	0.0099	66.7374	0.0126
71.75	71.7542	-0.0042	71.7502	-0.0002	71.7540	-0.0040	71.7543	-0.0043	71.7556	-0.0056
76.75	76.7509	-0.0009	76.7501	-0.0001	76.7511	-0.0011	76.7509	-0.0009	76.7510	-0.0010
81.75	81.7505	-0.0005	81.7505	-0.0005	81.7508	-0.0008	81.7504	-0.0004	81.7488	0.0012
86.75	86.7506	-0.0006	86.7503	-0.0003	86.7532	-0.0032	86.7504	-0.0004	86.7463	0.0037
91.75	91.7471	0.0029	91.7460	0.0040	91.7500	0.0000	91.7469	0.0031	91.7443	0.0057
96.75	96.7511	-0.0011	96.7501	-0.0001	96.7509	-0.0009	96.7512	-0.0012	96.7520	-0.0020

TABLE 16. Actual and predicted fault location with error during AC-G fault at line 8-9.

Actual Fault Location (km)	Predicted Fault Location (km) and Error for different Test cases									
	Test - I	Error	Test - II	Error	Test - III	Error	Test - IV	Error	Test - V	Error
1.6	1.5910	0.0090	1.5910	0.0090	1.5890	0.0110	1.6054	-0.0054	1.5884	0.0116
6.6	6.6021	-0.0021	6.6021	-0.0021	6.6109	-0.0109	6.5993	0.0007	6.3205	0.2795
11.6	11.6008	-0.0008	11.6008	-0.0008	11.5915	0.0085	11.6061	-0.0061	11.5245	0.0755
16.6	16.6015	-0.0015	16.6015	-0.0015	16.5892	0.0108	16.5938	0.0062	16.6141	-0.0141
21.6	21.5992	0.0008	21.5992	0.0008	21.5857	0.0143	21.5888	0.0112	21.7116	-0.1116
26.6	26.5990	0.0010	26.5990	0.0010	26.5883	0.0117	26.5872	0.0128	26.7682	-0.1682
31.6	31.5991	0.0009	31.5991	0.0009	31.5933	0.0067	31.5905	0.0095	31.7856	-0.1856
36.6	36.5997	0.0003	36.5997	0.0003	36.5982	0.0018	36.5799	0.0201	36.7710	-0.1710
41.6	41.6001	-0.0001	41.6001	-0.0001	41.6017	-0.0017	41.6014	-0.0014	41.7317	-0.1317
46.6	46.6004	-0.0004	46.6004	-0.0004	46.6041	-0.0041	46.5868	0.0132	46.6718	-0.0718
51.6	51.6006	-0.0006	51.6006	-0.0006	51.6042	-0.0042	51.5911	0.0089	51.6016	-0.0016
56.6	56.6005	-0.0005	56.6005	-0.0005	56.6022	-0.0022	56.5683	0.0317	56.5275	0.0725
61.6	61.6003	-0.0003	61.6003	-0.0003	61.5986	0.0014	61.5993	0.0007	61.4572	0.1428
66.6	66.6001	-0.0001	66.6001	-0.0001	66.5946	0.0054	66.5725	0.0275	66.4004	0.1996
71.6	71.5998	0.0002	71.5998	0.0002	71.5905	0.0095	71.5979	0.0021	71.3664	0.2336
76.6	76.5997	0.0003	76.5997	0.0003	76.5872	0.0128	76.5863	0.0137	76.3632	0.2368
81.6	81.5996	0.0004	81.5996	0.0004	81.5863	0.0137	81.5864	0.0136	81.4024	0.1976
86.6	86.5997	0.0003	86.5997	0.0003	86.5885	0.0115	86.5854	0.0146	86.4940	0.1060
91.6	91.6000	0.0000	91.6000	0.0000	91.5952	0.0048	91.5870	0.0130	91.6498	-0.0498
96.6	96.6003	-0.0003	96.6003	-0.0003	96.6071	-0.0071	96.5892	0.0108	96.8816	-0.2816

proposed scheme is shown in Figure 4. The initial weights and biases are generated randomly and are used to create the WNN output in step 1 [51]. Step 2 involves calculating the error value by subtracting the predicted output from

TABLE 17. Actual and predicted fault location with error during B-G fault at line 4-5.

Actual Fault Location (km)	Predicted Fault Location (km) and Error for different Test cases									
	Test - I	Error	Test - II	Error	Test - III	Error	Test - IV	Error	Test - V	Error
1.6	1.5893	0.0107	1.5893	0.0107	1.5385	0.0615	1.5683	0.0317	1.6213	-0.0213
6.6	6.5980	0.0020	6.5980	0.0020	6.5380	0.0620	6.5713	0.0287	6.5906	0.0094
11.6	11.6021	-0.0021	11.6021	-0.0021	11.5281	0.0719	11.5689	0.0311	11.5952	0.0048
16.6	16.5936	0.0064	16.5936	0.0064	16.5424	0.0576	16.5883	0.0117	16.5638	0.0362
21.6	21.6157	-0.0157	21.6157	-0.0157	21.5600	0.0400	21.6007	-0.0007	21.5756	0.0244
26.6	26.5969	0.0031	26.5969	0.0031	26.5356	0.0644	26.5796	0.0204	26.5608	0.0392
31.6	31.6005	-0.0005	31.6005	-0.0005	31.5249	0.0751	31.5834	0.0166	31.5602	0.0398
36.6	36.5978	0.0022	36.5978	0.0022	36.5273	0.0727	36.5831	0.0169	36.5319	0.0681
41.6	41.5978	0.0022	41.5978	0.0022	41.5288	0.0712	41.5857	0.0143	41.5446	0.0554
46.6	46.5990	0.0010	46.5990	0.0010	46.5315	0.0685	46.5886	0.0114	46.5708	0.0292
51.6	51.5997	0.0003	51.5997	0.0003	51.5337	0.0663	51.5903	0.0097	51.5753	0.0247
56.6	56.6012	-0.0012	56.6012	-0.0012	56.5382	0.0618	56.5933	0.0067	56.5487	0.0513
61.6	61.6017	-0.0017	61.6017	-0.0017	61.5417	0.0583	61.5949	0.0051	61.5322	0.0678
66.6	66.6018	-0.0018	66.6018	-0.0018	66.5450	0.0550	66.5956	0.0044	66.5467	0.0533
71.6	71.6012	-0.0012	71.6012	-0.0012	71.5478	0.0522	71.5953	0.0047	71.5563	0.0437
76.6	76.6001	-0.0001	76.6001	-0.0001	76.5502	0.0498	76.5942	0.0058	76.5541	0.0459
81.6	81.5988	0.0012	81.5988	0.0012	81.5525	0.0475	81.5925	0.0075	81.5616	0.0384
86.6	86.5978	0.0022	86.5978	0.0022	86.5553	0.0447	86.5911	0.0089	86.5603	0.0397
91.6	91.5983	0.0017	91.5983	0.0017	91.5595	0.0405	91.5910	0.0090	91.5566	0.0434
96.6	96.6015	-0.0015	96.6015	-0.0015	96.5666	0.0334	96.5936	0.0064	96.5385	0.0615

TABLE 18. Actual and predicted fault location with error during BC fault at line 4-5.

Actual Fault Location (km)	Predicted Fault Location (km) and Error for different Test cases									
	Test - I	Error	Test - II	Error	Test - III	Error	Test - IV	Error	Test - V	Error
1.45	1.4502	-0.0002	1.4365	0.0135	1.4329	0.0171	1.4466	0.0034	1.4128	0.0372
6.45	6.4486	0.0014	6.4265	0.0235	6.4219	0.0281	6.4373	0.0127	6.4064	0.0436
11.45	11.4489	0.0011	11.4315	0.0185	11.4268	0.0232	11.4396	0.0104	11.4281	0.0219
16.45	16.4659	-0.0159	16.4239	0.0261	16.3910	0.0590	16.4324	0.0176	16.4414	0.0086
21.45	21.4428	0.0072	21.4195	0.0305	21.4293	0.0207	21.3912	0.0588	21.1068	0.3432
26.45	26.4463	0.0037	26.3916	0.0584	26.3674	0.0826	26.4185	0.0315	26.4311	0.0189
31.45	31.4485	0.0015	31.3855	0.0645	31.3678	0.0822	31.4110	0.0390	31.4335	0.0165
36.45	36.4490	0.0010	36.3766	0.0734	36.3592	0.0908	36.4013	0.0487	36.4423	0.0077
41.45	41.4512	-0.0012	41.3696	0.0804	41.3471	0.1029	41.3989	0.0511	41.4511	-0.0011
46.45	46.4530	-0.0030	46.3627	0.0873	46.3389	0.1111	46.3945	0.0555	46.4593	-0.0093
51.45	51.4529	-0.0029	51.3568	0.0932	51.3306	0.1194	51.3887	0.0613	51.4629	-0.0129
56.45	56.4516	-0.0016	56.3517	0.0983	56.3225	0.1275	56.3851	0.0649	56.4630	-0.0130
61.45	61.4498	0.0002	61.3462	0.1038	61.3153	0.1347	61.3806	0.0694	61.4605	-0.0105
66.45	66.4481	0.0019	66.3415	0.1085	66.3084	0.1416	66.3765	0.0735	66.4560	-0.0060
71.45	71.4475	0.0025	71.3375	0.1125	71.3021	0.1479	71.3733	0.0767	71.4496	0.0004
76.45	76.4482	0.0018	76.3340	0.1160	76.2964	0.1536	76.3703	0.0797	76.4420	0.0080
81.45	81.4500	0.0000	81.3310	0.1190	81.2911	0.1589	81.3676	0.0824	81.4330	0.0170
86.45	86.4520	-0.0020	86.3285	0.1215	86.2864	0.1636	86.3651	0.0849	86.4216	0.0284
91.45	91.4526	-0.0026	91.3263	0.1237	91.2820	0.1680	91.3630	0.0870	91.4063	0.0437
96.45	96.4492	0.0008	96.3242	0.1258	96.2778	0.1722	96.3609	0.0891	96.3846	0.0654

the actual output. Step 3 involves adjusting the initialized weights in all links and biases in all neurons to minimize the error by propagating the error backward. In this regard, the limited-memory Broyden, Fletcher, Goldfarb, and Shanno

TABLE 19. Actual and predicted fault location with error during BC-G fault at line 4-5.

Actual Fault Location (km)	Predicted Fault Location (km) and Error for different Test cases									
	Test - I	Error	Test - II	Error	Test - III	Error	Test - IV	Error	Test - V	Error
4.75	4.7534	-0.0034	4.7563	-0.0063	4.7379	0.0121	4.7550	-0.0050	4.7550	-0.0050
9.75	9.7507	-0.0007	9.7481	0.0019	9.7483	0.0017	9.7487	0.0013	9.7497	0.0003
14.75	14.7494	0.0006	14.7408	0.0092	14.7379	0.0121	14.7481	0.0019	14.7887	-0.0387
19.75	19.7474	0.0026	19.7418	0.0082	19.7544	-0.0044	19.7342	0.0158	19.7342	0.0158
24.75	24.7488	0.0012	24.7451	0.0049	24.7470	0.0030	24.7400	0.0100	24.7400	0.0100
29.75	29.7506	-0.0006	29.7508	-0.0008	29.7638	-0.0138	29.7435	0.0065	29.7434	0.0066
34.75	34.7515	-0.0015	34.7533	-0.0033	34.7443	0.0057	34.7482	0.0018	34.7482	0.0018
39.75	39.7518	-0.0018	39.7572	-0.0072	39.7491	0.0009	39.7533	-0.0033	39.7533	-0.0033
44.75	44.7515	-0.0015	44.7586	-0.0086	44.7471	0.0029	44.7549	-0.0049	44.7549	-0.0049
49.75	49.7507	-0.0007	49.7583	-0.0083	49.7552	-0.0052	49.7540	-0.0040	49.7540	-0.0040
54.75	54.7496	0.0004	54.7558	-0.0058	54.7405	0.0095	54.7536	-0.0036	54.7536	-0.0036
59.75	59.7489	0.0011	59.7532	-0.0032	59.7527	-0.0027	59.7507	-0.0007	59.7507	-0.0007
64.75	64.7486	0.0014	64.7494	0.0006	64.7518	-0.0018	64.7473	0.0027	64.7473	0.0027
69.75	69.7487	0.0013	69.7457	0.0043	69.7324	0.0176	69.7443	0.0057	69.7443	0.0057
74.75	74.7494	0.0006	74.7430	0.0070	74.7645	-0.0145	74.7422	0.0078	74.7422	0.0078
79.75	79.7503	-0.0003	79.7418	0.0082	79.7410	0.0090	79.7413	0.0087	79.7413	0.0087
84.75	84.7512	-0.0012	84.7426	0.0074	84.7660	-0.0160	84.7424	0.0076	84.7424	0.0076
89.75	89.7513	-0.0013	89.7460	0.0040	89.7405	0.0095	89.7465	0.0035	89.7465	0.0035
94.75	94.7502	-0.0002	94.7523	-0.0023	94.7760	-0.0260	94.7533	-0.0033	94.7533	-0.0033

TABLE 20. Actual and predicted fault location with error during A-G fault at line 7-8.

Actual Fault Location (km)	Predicted Fault Location (km) and Error for different Test cases									
	Test - I	Error	Test - II	Error	Test - III	Error	Test - IV	Error	Test - V	Error
1.5	1.4980	0.0020	1.4980	0.0020	1.4976	0.0024	1.4981	0.0019	1.4972	0.0028
6.5	6.5025	-0.0025	6.5025	-0.0025	6.4988	0.0012	6.5000	0.0000	6.5013	-0.0013
11.5	11.4984	0.0016	11.4984	0.0016	11.4965	0.0035	11.4973	0.0027	11.5005	-0.0005
16.5	16.4929	0.0071	16.4929	0.0071	16.4934	0.0066	16.4933	0.0067	16.4938	0.0062
21.5	21.4957	0.0043	21.4957	0.0043	21.5160	-0.0160	21.5179	-0.0179	21.5379	-0.0379
26.5	26.5024	-0.0024	26.5024	-0.0024	26.5021	-0.0021	26.5019	-0.0019	26.4971	0.0029
31.5	31.5027	-0.0027	31.5027	-0.0027	31.5034	-0.0034	31.5030	-0.0030	31.5008	-0.0008
36.5	36.5031	-0.0031	36.5031	-0.0031	36.5036	-0.0036	36.5035	-0.0035	36.5032	-0.0032
41.5	41.5028	-0.0028	41.5028	-0.0028	41.5034	-0.0034	41.5034	-0.0034	41.5028	-0.0028
46.5	46.5015	-0.0015	46.5015	-0.0015	46.5021	-0.0021	46.5021	-0.0021	46.5014	-0.0014
51.5	51.4999	0.0001	51.4999	0.0001	51.5003	-0.0003	51.5002	-0.0002	51.4997	0.0003
56.5	56.4980	0.0020	56.4980	0.0020	56.4985	0.0015	56.4985	0.0015	56.4982	0.0018
61.5	61.4969	0.0031	61.4969	0.0031	61.4974	0.0026	61.4974	0.0026	61.4971	0.0029
66.5	66.4968	0.0032	66.4968	0.0032	66.4971	0.0029	66.4971	0.0029	66.4970	0.0030
71.5	71.4978	0.0022	71.4978	0.0022	71.4980	0.0020	71.4980	0.0020	71.4979	0.0021
76.5	76.4998	0.0002	76.4998	0.0002	76.4999	0.0001	76.4999	0.0001	76.4998	0.0002
81.5	81.5021	-0.0021	81.5021	-0.0021	81.5021	-0.0021	81.5021	-0.0021	81.5022	-0.0022
86.5	86.5037	-0.0037	86.5037	-0.0037	86.5036	-0.0036	86.5036	-0.0036	86.5038	-0.0038
91.5	91.5030	-0.0030	91.5030	-0.0030	91.5028	-0.0028	91.5028	-0.0028	91.5030	-0.0030
96.5	96.4975	0.0025	96.4975	0.0025	96.4973	0.0027	96.4973	0.0027	96.4976	0.0024

(L-BFGS) back-propagation algorithm [52], [53], [54] is used during the back-propagation process. The L-BFGS is used to solve high-dimensional minimization problems when the objective function and its gradient can be calculated

TABLE 21. Actual and predicted fault location with error during AB fault at line 7-8.

Actual Fault Location (km)	Predicted Fault Location (km) and Error for different Test cases									
	Test - I	Error	Test - II	Error	Test - III	Error	Test - IV	Error	Test - V	Error
3.25	3.2527	-0.0027	3.2562	-0.0062	3.2553	-0.0053	3.2496	0.0004	3.2551	-0.0051
8.25	8.2463	0.0037	8.2829	-0.0329	8.2422	0.0078	8.2573	-0.0073	8.2669	-0.0169
13.25	13.2558	-0.0058	13.2556	-0.0056	13.2631	-0.0131	13.2540	-0.0040	13.2515	-0.0015
18.25	18.2451	0.0049	18.2489	0.0011	18.2501	-0.0001	18.2477	0.0023	18.2535	-0.0035
23.25	23.2585	-0.0085	23.2412	0.0088	23.2567	-0.0067	23.2550	-0.0050	23.2419	0.0081
28.25	28.2473	0.0027	28.2443	0.0057	28.2579	-0.0079	28.2588	-0.0088	28.2546	-0.0046
33.25	33.2483	0.0017	33.2459	0.0041	33.2391	0.0109	33.2491	0.0009	33.2482	0.0018
38.25	38.2500	0.0000	38.2468	0.0032	38.2495	0.0005	38.2518	-0.0018	38.2484	0.0016
43.25	43.2525	-0.0025	43.2487	0.0013	43.2485	0.0015	43.2542	-0.0042	43.2500	0.0000
48.25	48.2536	-0.0036	48.2499	0.0001	48.2494	0.0006	48.2547	-0.0047	48.2506	-0.0006
53.25	53.2530	-0.0030	53.2493	0.0007	53.2508	-0.0008	53.2540	-0.0040	53.2501	-0.0001
58.25	58.2512	-0.0012	58.2482	0.0018	58.2570	-0.0070	58.2515	-0.0015	58.2489	0.0011
63.25	63.2491	0.0009	63.2463	0.0037	63.2418	0.0082	63.2485	0.0015	63.2461	0.0039
68.25	68.2474	0.0026	68.2451	0.0049	68.2561	-0.0061	68.2464	0.0036	68.2444	0.0056
73.25	73.2469	0.0031	73.2453	0.0047	73.2494	0.0006	73.2448	0.0052	73.2452	0.0048
78.25	78.2482	0.0018	78.2473	0.0027	78.2454	0.0046	78.2456	0.0044	78.2464	0.0036
83.25	83.2506	-0.0006	83.2517	-0.0017	83.2544	-0.0044	83.2475	0.0025	83.2510	-0.0010
88.25	88.2533	-0.0033	88.2556	-0.0056	88.2519	-0.0019	88.2493	0.0007	88.2535	-0.0035
93.25	93.2532	-0.0032	93.2556	-0.0056	93.2485	0.0015	93.2478	0.0022	93.2542	-0.0042
98.25	98.2450	0.0050	98.2492	0.0008	98.2517	-0.0017	98.2389	0.0111	98.2466	0.0034

TABLE 22. Actual and predicted fault location with error during ABC fault at line 7-8.

Actual Fault Location (km)	Predicted Fault Location (km) and Error for different Test cases									
	Test - I	Error	Test - II	Error	Test - III	Error	Test - IV	Error	Test - V	Error
4.75	4.7606	-0.0106	4.7605	-0.0105	4.7590	-0.0090	4.7290	0.0210	4.7479	0.0021
9.75	9.7641	-0.0141	9.7643	-0.0143	9.6868	0.0632	9.7536	-0.0036	9.7602	-0.0102
14.75	14.7503	-0.0003	14.7502	-0.0002	14.7056	0.0444	14.7278	0.0222	14.7603	-0.0103
19.75	19.7411	0.0089	19.7413	0.0087	19.7640	-0.0140	19.7157	0.0343	19.7563	-0.0063
24.75	24.7488	0.0012	24.7478	0.0022	24.7462	0.0038	24.7105	0.0395	24.7526	-0.0026
29.75	29.7418	0.0082	29.7418	0.0082	29.7498	0.0002	29.7025	0.0475	29.7510	-0.0010
34.75	34.7433	0.0067	34.7433	0.0067	34.7487	0.0013	34.7016	0.0484	34.7506	-0.0006
39.75	39.7480	0.0020	39.7480	0.0020	39.7473	0.0027	39.7030	0.0470	39.7508	-0.0008
44.75	44.7526	-0.0026	44.7526	-0.0026	44.7502	-0.0002	44.7059	0.0441	44.7527	-0.0027
49.75	49.7562	-0.0062	49.7562	-0.0062	49.7561	-0.0061	49.7090	0.0410	49.7548	-0.0048
54.75	54.7584	-0.0084	54.7584	-0.0084	54.7463	0.0037	54.7130	0.0370	54.7570	-0.0070
59.75	59.7594	-0.0094	59.7594	-0.0094	59.7510	-0.0010	59.7207	0.0293	59.7580	-0.0080
64.75	64.7561	-0.0061	64.7561	-0.0061	64.7501	-0.0001	64.7122	0.0378	64.7589	-0.0089
69.75	69.7531	-0.0031	69.7531	-0.0031	69.7548	-0.0048	69.7130	0.0370	69.7596	-0.0096
74.75	74.7490	0.0010	74.7490	0.0010	74.7441	0.0059	74.7087	0.0413	74.7582	-0.0082
79.75	79.7451	0.0049	79.7451	0.0049	79.7530	-0.0030	79.7075	0.0425	79.7578	-0.0078
84.75	84.7429	0.0071	84.7429	0.0071	84.7473	0.0027	84.7066	0.0434	84.7555	-0.0055
89.75	89.7440	0.0060	89.7440	0.0060	89.7503	-0.0003	89.7092	0.0408	89.7530	-0.0030
94.75	94.7499	0.0001	94.7499	0.0001	94.7526	-0.0026	94.7158	0.0342	94.7501	-0.0001

analytically [53]. The network outputs (predicted FL) and error are computed again with the adapted weights and biases, and the procedure (WNN training) is continued until a satisfying FL output y_1 is obtained corresponding to the

TABLE 23. Actual and predicted fault location with error during AB-G fault at line 7-8.

Actual Fault Location (km)	Predicted Fault Location (km) and Error for different Test cases									
	Test - I	Error	Test - II	Error	Test - III	Error	Test - IV	Error	Test - V	Error
2.5	2.5134	-0.0134	2.5134	-0.0134	2.5020	-0.0020	2.5019	-0.0019	2.5309	-0.0309
6.5	6.5002	-0.0002	6.5002	-0.0002	6.5061	-0.0061	6.5234	-0.0234	6.5089	-0.0089
10.5	10.4940	0.0060	10.4940	0.0060	10.5026	-0.0026	10.5011	-0.0011	10.5099	-0.0099
14.5	14.5001	-0.0001	14.5001	-0.0001	14.4921	0.0079	14.5098	-0.0098	14.5199	-0.0199
18.5	18.4988	0.0012	18.4988	0.0012	18.4912	0.0088	18.4964	0.0036	18.5106	-0.0106
22.5	22.5020	-0.0020	22.5020	-0.0020	22.4855	0.0145	22.4905	0.0095	22.5192	-0.0192
26.5	26.5018	-0.0018	26.5018	-0.0018	26.4918	0.0082	26.4964	0.0036	26.5133	-0.0133
30.5	30.5021	-0.0021	30.5021	-0.0021	30.4906	0.0094	30.4977	0.0023	30.5190	-0.0190
34.5	34.5016	-0.0016	34.5016	-0.0016	34.4953	0.0047	34.5049	-0.0049	34.5163	-0.0163
38.5	38.5020	-0.0020	38.5020	-0.0020	38.4984	0.0016	38.5019	-0.0019	38.5173	-0.0173
42.5	42.5013	-0.0013	42.5013	-0.0013	42.5035	-0.0035	42.4980	0.0020	42.5137	-0.0137
46.5	46.5000	0.0000	46.5000	0.0000	46.5060	-0.0060	46.5026	-0.0026	46.5111	-0.0111
50.5	50.4993	0.0007	50.4993	0.0007	50.5074	-0.0074	50.4902	0.0098	50.5083	-0.0083
54.5	54.4994	0.0006	54.4994	0.0006	54.5065	-0.0065	54.5082	-0.0082	54.5061	-0.0061
58.5	58.4993	0.0007	58.4993	0.0007	58.5052	-0.0052	58.5243	-0.0243	58.5043	-0.0043
62.5	62.4985	0.0015	62.4985	0.0015	62.5042	-0.0042	62.4793	0.0207	62.5049	-0.0049
66.5	66.4982	0.0018	66.4982	0.0018	66.4994	0.0006	66.4963	0.0037	66.5005	-0.0005
70.5	70.4990	0.0010	70.4990	0.0010	70.4942	0.0058	70.5196	-0.0196	70.5002	-0.0002
74.5	74.4999	0.0001	74.4999	0.0001	74.4920	0.0080	74.4927	0.0073	74.4982	0.0018
78.5	78.5001	-0.0001	78.5001	-0.0001	78.4892	0.0108	78.4888	0.0112	78.4976	0.0024
82.5	82.5011	-0.0011	82.5011	-0.0011	82.4879	0.0121	82.5187	-0.0187	82.4964	0.0036
86.5	86.5013	-0.0013	86.5013	-0.0013	86.4905	0.0095	86.4963	0.0037	86.4952	0.0048
90.5	90.5011	-0.0011	90.5011	-0.0011	90.4958	0.0042	90.4875	0.0125	90.4932	0.0068
94.5	94.5001	-0.0001	94.5001	-0.0001	94.5069	-0.0069	94.5105	-0.0105	94.4908	0.0092
98.5	98.4978	0.0022	98.4978	0.0022	98.5231	-0.0231	98.4855	0.0145	98.4872	0.0128

values of the input variables x and the error is acceptably small.

IV. RESULTS AND DISCUSSION

This section discusses the performance of the proposed FL estimator for different types of faults occurring in various TL sections of the considered power system.

A. PERFORMANCE OF THE PROPOSED FAULT LOCATOR FOR VARIOUS FAULTS

Table 4 shows the various performance metrics of the proposed FL estimator for single line to ground fault (C-G) at lines 8-9. The performance metrics are compared with other ML algorithms such as DT and SVM. Concerning Table 1, different test cases are considered for C-G fault in the same line section. The FL for test cases lies between 3.25 km and 95.25 km with a step size of 4 km. The FIAs for 5 test cases is 0°, 15°, 45°, 75°, and 105° respectively. The performance metrics are analyzed for both training and testing datasets. Table 4 shows that the WNN-based proposed fault locator identifies the FL with minimum error compared with other ML algorithms. The various performance metrics, such as MAE, MSE, and RMSE, clearly show the effectiveness of the proposed FL scheme for both training and testing. Similarly, the error metrics are calculated for AC and AC-G faults in line sections 8-9 and are presented in Table 5 and Table 6, respectively.

In addition, TLs 4-5 and 7-8 are considered for the FL estimation problems. In TL sections IV-V, three different types of faults (B-G fault, BC fault, and BC-G fault) are considered with three different sets of FIAs for testing the proposed scheme. For every test case, the fault locations are also modified. The performance metrics for both training and test cases are shown in Table 7-9 for the above-mentioned faults. In TL 7-8, different types of faults such as A-G fault, AB fault, ABC fault, and AB-G fault are considered for FL estimation problem. The performance metrics of the proposed FL estimation scheme are shown in Table 10-13 for the aforementioned faults in lines 7-8. Table 4-13 show that, for all the fault types with different test cases, the proposed fault locator identifies the FL with lesser error than other techniques. The performance metrics for various faults on FL are used to calculate the estimated FD from the relay point. In this regard, the percentage FL error and the absolute

TABLE 24. Performance of the proposed scheme with different features during C-G fault at line 8-9.

Results	Metrics	Features Considered		
		Voltage, Current, Phase angle	Voltage Magnitude Alone	Current Magnitude Alone
Training	MAE	0.00367	0.07233	0.09900
	MSE	0.00002	0.01848	0.01654
	RMSE	0.00470	0.13593	0.12861
Test I	MAE	0.00368	0.07792	0.09937
	MSE	0.00002	0.02286	0.01652
	RMSE	0.00476	0.15120	0.12853
Test II	MAE	0.00548	0.09042	0.16902
	MSE	0.00005	0.02166	0.05252
	RMSE	0.00703	0.14717	0.22916
Test III	MAE	0.00902	0.10060	0.28973
	MSE	0.00013	0.01660	0.15449
	RMSE	0.01115	0.12883	0.39305
Test IV	MAE	0.01017	0.10104	0.32771
	MSE	0.00017	0.01427	0.19607
	RMSE	0.01294	0.11946	0.44280
Test V	MAE	0.00873	0.10421	0.27898
	MSE	0.00012	0.01846	0.14187
	RMSE	0.01117	0.13587	0.37666

average error percentage of FL are calculated using Eq. (9) and Eq. (10) [15].

$$Error_k(\%) = \frac{(A_k - P_k)}{L} \times 100 \tag{9}$$

$$Absolute\ average\ error(\%) = \left| \frac{\sum_{k=1}^{T} Error_k(\%)}{T} \right| \tag{10}$$

where, $Error_k(\%)$ is the k^{th} error(%), L is the total line length, and T is the number of input data. For illustration, consider the C-G fault in lines 8-9. Table 14 shows the actual and predicted FL with an error during the C-G fault at lines 8-9. The average FL is estimated for 24 different fault locations lies between 3.25 km and 95.25 km with a uniform step size of 4 km. The negative sign in the error indicates that the estimated FL is greater than the actual FL. It is inferred from Table 14 that the error in the predicted FL is lesser and is in the order of 10^{-2} to 10^{-3}. Furthermore, the average prediction error for the C-G fault in lines 8-9 has been calculated, resulting in an error value of 0.0095. It shows the effectiveness of the proposed WNN-based fault locator. Figure 5 shows the residuals in predicted FL for the C-G fault in line sections 8-9. It indicates the error range for all the fault locations of each test case. Figure 5(a) shows the residuals in predicted FL for test case I with a FIA of 0°. It is clear that the aforementioned fault locations lies between 3.25 km and 95.25 km with a step size of 4 km and have a minimum error range.

Similarly, Figure 5(b)-5(e) show the error analysis for the rest of the test cases with FIAs of 15°, 45°, 75°, and 105°, respectively. It is observed from Figure 5(a)-5(e) that the residuals and their range for all the test cases are lesser. In addition to Table 14, Figure 5 describes the performance of the proposed fault locator with detailed residual analysis. Similarly, the line-to-line fault (AC) and double line-to-ground (AC-G) fault in lines section 8-9 are considered, and the actual and predicted FL with errors are shown in Table 15 and Table 16, respectively, for the aforementioned faults. In addition, the line-to-line (AC) fault is considered for the analysis of residuals in predicted FL for different test cases and is shown in Figure 6(a)-6(e). It is inferred from Table 15 and Figure 6 that the proposed fault locator estimates the FL with an error of ±0.03. This shows the efficacy of the proposed fault locator. Similarly, Table 16 shows the actual and predicted FL for the AC-G fault. Additionally, to demonstrate the accuracy of the proposed scheme, the average prediction errors for line-to-line (AC) and double line-to-ground (AC-G) faults have been calculated, yielding error values of 0.0032 and 0.032, respectively.

The errors in the FL for different types of faults, such as B-G fault, BC fault, and BC-G fault on TL 4-5, are presented in Table 17-19, respectively. The aforementioned tables show the effectiveness of the proposed fault locator in estimating

TABLE 25. Performance of the proposed scheme with different features during BC-G fault at line 4-5.

Results	Metrics	Features Considered		
		Voltage, Current and Phase angle	Voltage Magnitude Alone	Current Magnitude Alone
Training	MAE	0.00794	0.06391	0.21840
	MSE	0.00016	0.00613	0.07498
	RMSE	0.01261	0.07828	0.27382
Test I	MAE	0.00678	0.06208	0.18940
	MSE	0.00011	0.00570	0.05967
	RMSE	0.01065	0.07553	0.24428
Test II	MAE	0.07174	0.28057	2.23220
	MSE	0.00741	0.10897	7.01130
	RMSE	0.08607	0.33010	2.64790
Test III	MAE	0.07419	0.09351	4.06510
	MSE	0.00985	0.01593	23.34400
	RMSE	0.09924	0.12620	4.83160
Test IV	MAE	0.02560	0.08680	3.48790
	MSE	0.00141	0.01198	17.06400
	RMSE	0.03780	0.28686	4.13090
Test V	MAE	0.02583	0.06841	0.33549
	MSE	0.00142	0.00832	0.28403
	RMSE	0.03771	0.09121	0.53294

TABLE 26. Performance of the proposed scheme with different features during AB fault at line 7-8.

Results	Metrics	Features Considered		
		Voltage, Current, Phase angle	Voltage Magnitude Alone	Current Magnitude Alone
Training	MAE	0.02226	0.11516	0.21766
	MSE	0.00190	0.02169	0.08107
	RMSE	0.04362	0.14728	0.28472
Test I	MAE	0.02280	0.12485	0.21766
	MSE	0.00188	0.02704	0.08107
	RMSE	0.04331	0.16444	0.28472
Test II	MAE	0.03896	0.20479	0.30533
	MSE	0.00593	0.10900	0.15838
	RMSE	0.07700	0.33016	0.39798
Test III	MAE	0.04507	0.27433	0.47827
	MSE	0.00636	0.24146	0.36154
	RMSE	0.07977	0.49138	0.60128
Test IV	MAE	0.03198	0.13280	0.24334
	MSE	0.00257	0.02971	0.10181
	RMSE	0.05068	0.17235	0.31908
Test V	MAE	0.05421	0.26985	0.26348
	MSE	0.00973	0.19061	0.13177
	RMSE	0.09863	0.43659	0.36300

the FL. For illustration, the residuals in the predicted FL for single line to ground (B-G) fault on TL 4-5 with different test cases are shown in Figure 7(a)-7(e). Similarly, four different types of faults (A-G fault, AB fault, ABC fault, and AB-G

TABLE 27. Performance of the proposed scheme with different features during ABC fault at line 7-8.

Results	Metrics	Features Considered		
		Voltage, Current, Phase angle	Voltage Magnitude Alone	Current Magnitude Alone
Training	MAE	0.00957	0.05683	0.49773
	MSE	0.00025	0.00573	0.45244
	RMSE	0.01593	0.07572	0.67263
Test I	MAE	0.01056	0.05940	0.13370
	MSE	0.00033	0.00603	0.07313
	RMSE	0.01818	0.07763	0.27042
Test II	MAE	0.02571	0.71865	2.06980
	MSE	0.02216	0.75191	5.50290
	RMSE	0.04707	0.86713	2.34580
Test III	MAE	0.14163	1.76240	2.75080
	MSE	0.03179	4.50260	9.73500
	RMSE	0.17829	2.12190	3.12010
Test IV	MAE	0.08387	1.82400	3.26230
	MSE	0.01135	4.88300	3.64400
	RMSE	0.10652	2.20980	3.69380
Test V	MAE	0.08481	0.61287	2.39020
	MSE	0.01295	0.54266	7.29110
	RMSE	0.11380	0.73665	2.70020

TABLE 28. Average absolute prediction error in fault location.

Techniques	Type of fault			
	LG	LL	LLG	LLL
ANFIS [31]	0.6314	0.4871	0.7508	NA
ANN [31]	0.9042	1.5564	0.5407	NA
DWT-ANFIS [31]	0.1833	0.2028	0.1208	NA
DGNN [41]	0.4442			
Proposed	**0.0121**	**0.0209**	**0.0139**	**0.0124**

TABLE 29. Average training and testing performance.

Techniques	Training		Testing	
	MAE	RMSE	MAE	RMSE
ANN [31]	2.6640	4.2290	3.2710	5.1710
ANFIS [31]	0.6640	1.1180	1.1420	1.8800
DWT-ANFIS [31]	2.1910	7.1990	2.1610	7.2340
SOM [31]	0.0510	1.1290	3.6690	14.7440
Proposed	**0.0109**	**0.0192**	**0.0390**	**0.0566**

fault) are considered in TL 7-8, with four different sets of FIAs for each type of fault, respectively. To show the efficacy of the proposed scheme, the performance metrics on the FL are shown in Table 20-23 for the above-said faults. For illustration, the residuals in the predicted FL for different test cases are shown in Figure 8(a)-8(e) for line-to-line (AB) fault on TL 7-8. It is observed from Table 20-23 and Figure 8 that the proposed fault locator effectively identifies the FL with lesser error. To demonstrate the effectiveness of the proposed fault locator, the prediction errors for fault localization can be calculated for all faults discussed in Tables 17 through 23. The overall prediction errors for LG, LL, LL-G, and LLL faults are calculated and discussed in subsection C.

B. COMPARATIVE ANALYSIS OF PERFORMANCE METRICS OF THE PROPOSED SCHEME WITH DIFFERENT FEATURES

Table 24 presents a comparative analysis of the performance metrics for the proposed FL scheme when applied to a single line-to-ground (C-G) fault on lines 8-9. This analysis examines input features, including voltage and current magnitudes with phase angle, voltage magnitude alone, and current magnitude alone. The percentage reductions in MAE, MSE, and RMSE for Test I are also calculated for demonstration. Specifically, the percentage reduction in MAE when all three features are considered is compared with voltage magnitude, and current magnitude alone is considered as a feature set. The MAE reductions are 95.27% and 96.29%, respectively, while MSE reductions are 99.90% and 99.86%, and RMSE reductions are 96.85% and 96.23% for voltage and current alone, respectively. Similarly, the percentage reductions in these performance metrics for the other test cases can be calculated. Table 24 illustrates that including phase angle as a feature set significantly enhances the accuracy of the estimated fault location compared to rest of the feature sets with voltage and current magnitude alone. Correspondingly, Table 25-27 detail the performance metrics for the proposed

FL estimation scheme for different fault types, such as double line-to-ground (BC-G) fault on lines 4-5, line-to-line (AB) fault on lines 7-8, and triple line (ABC) fault on line 7-8, respectively. It is evident from Table 25-27 that incorporating phase angle in the input features consistently results in more accurate fault location identification with minimal error compared to using magnitude alone.

C. COMPARATIVE ANALYSIS WITH EXISTING TECHNIQUES

Table 28 presents a comparative analysis of the average absolute prediction error for transmission line fault localization. The different types of faults, such as L-G, LL, LL-G, and LLL faults, are considered for analysis. The proposed technique achieves the lowest prediction error for L-G faults at 0.0121. The prediction errors obtained for LL, LL-G, and LLL faults are 0.0209, 0.0139, and 0.0124, respectively. The DGNN technique yields an overall prediction error of 0.442 for all fault types. Notably, in all fault categories and localization, the proposed technique outperforms existing methods, such as ANFIS, ANN, DWT-ANFIS, and DGNN. Table 29 highlights the performance metrics of the proposed fault localization scheme compared to existing techniques, focusing on MAE and RMSE values for both the training and testing phases. The proposed technique records the lowest average MAE of 0.0109 and RMSE of 0.0192 during training. In testing, it also achieves the lowest MAE and RMSE values of 0.0390 and 0.0566, respectively. These results indicate that the proposed method performs better in training and testing than the other fault localization techniques.

V. CONCLUSION

In this paper, a WNN-based fault locator was developed for the WSCC 9-bus system using the MATLAB/Simulink environment. In addition, the optimal PMU placement is considered, ensuring PMUs are strategically placed to achieve 100% system observability. The WNN was trained using the PMU-derived features such as voltage and current magnitudes and phase angles to estimate the fault location by creating specific faults within the system. The analysis of prediction errors revealed absolute prediction errors of 0.0121 for L-G faults, 0.0209 for LL faults, 0.0139 for LL-G faults, and 0.0124 for LLL faults, demonstrating the effectiveness of the proposed fault locator compared with the existing techniques. Training and testing results indicated significant MAE, MSE, and RMSE reductions when incorporating voltage, current, and phase angle features. Specifically, the MAE is reduced by 95.27% and 96.29% compared to voltage and current alone, respectively. MSE reductions were 99.90% and 99.86%, while RMSE reductions were 96.85% and 96.23% for voltage and current alone, respectively. These results underscore the importance of including phase angle measurements to enhance fault location accuracy beyond using voltage and current magnitudes alone. The proposed WNN-based method was benchmarked against other regression-based models, such as decision trees and support vector machines, across various test scenarios at different fault locations. The performance metrics confirmed the superior accuracy of the WNN-based fault location scheme over other techniques. In future, the effect of frequency domain features can also be thought of with WNN for enhancing the performance of the proposed fault locator.

A. ABBREVIATIONS

AI	Artificial intelligence
ANFIS	Adaptive neuro-fuzzy inference system
ANN	Artificial neural networks
DGNN	Deep graph neural network
DL	Deep learning
DT	Decision tree
DTT	Digital twin technology
DWT-ANFIS	Discrete wavelet transform-Adaptive neurofuzzy inference system
EmHW	Embryonic hardware
FD	Fault distance
FF-ANNC	Firefly algorithm-trained ANN controller
FIA	Fault inception angle
FL	Fault location
FR	Fault resistance
GPS	Global positioning system
L-BFGS	Limited-memory Broyden, Fletcher, Goldfarb, and Shanno
L-G	Line-to-ground fault
LL	Line-to-line fault
LL-G	Double line-to-ground fault
LLL	Triple line fault
LLL-G	Triple line-to-ground fault
MAE	Mean absolute error
MATLAB	Matrix laboratory
ML	Machine learning
MSE	Mean squared error
OPP	Optimal PMU placement
PMU	Phasor measurement unit
PQ	Power quality
ReLU	Rectified linear unit
RMSE	Root mean squared error
SG	Smart grids
SOM	Self-organizing map
SPV	Solar photovoltaic
SVM	Support vector machine
TL	Transmission line
TLBO	Teaching-learning-based optimization
WAMS	Wide area monitoring system
WNN	Wide neural network
WSCC	Western system coordinating council

REFERENCES

[1] H. H. Sait, "Auditing and analysis of energy consumption of an educational building in hot and humid area," *Energy Convers. Manage.*, vol. 66, pp. 143–152, Feb. 2013.

[2] A. Mouco and A. Abur, "Improving the wide-area PMU-based fault location method using ordinary least squares estimation," *Electr. Power Syst. Res.*, vol. 189, Dec. 2020, Art. no. 106620.

[3] S. Jian, X. Peng, K. Wu, and H. Yuan, "Transmission line fault-cause classification based on multi-view sparse feature selection," *Energy Rep.*, vol. 8, pp. 614–621, Aug. 2022.
[4] J. Tejeswara Rao and B. R. Bhalja, "Prevention of maloperation of distance relay under severe stressed conditions for series compensated transmission line considering optimal placement of phasor measurement units," *IET Gener., Transmiss. Distrib.*, vol. 14, no. 11, pp. 2148–2159, Jun. 2020.
[5] A. Dwivedi, B. Mallikarjuna, D. Pal, M. J. B. Reddy, and D. K. Mohanta, "A real-time synchrophasor-based Zone-3 supervision of distance relays under load encroachment condition," *IEEE Syst. J.*, vol. 13, no. 4, pp. 4227–4235, Dec. 2019.
[6] A. Prasad, J. B. Edward, and K. Ravi, "A review on fault classification methodologies in power transmission systems: Part—I," *J. Elect. Syst. Inf. Technol.*, vol. 5, no. 1, pp. 48–60, 2018.
[7] H. Fathabadi, "Novel filter based ANN approach for short-circuit faults detection, classification and location in power transmission lines," *Int. J. Electr. Power Energy Syst.*, vol. 74, pp. 374–383, Jan. 2016.
[8] R. Mohammadi, M. Ghotbi-Maleki, and A. Ghaffarzadeh, "Wide-area fault location in transmission power system considering measurement uncertainty," *IEEE Access*, vol. 12, pp. 42535–42543, 2024.
[9] A. G. Phadke, J. S. Thorp, and K. J. Karimi, "State estimlatjon with phasor measurements," *IEEE Trans. Power Syst.*, vol. PWRS-1, no. 1, pp. 233–238, Feb. 1986.
[10] X. Zhou, Y. Wang, Y. Shi, Q. Jiang, C. Zhou, and Z. Zheng, "Deep reinforcement learning-based optimal PMU placement considering the degree of power system observability," *IEEE Trans. Ind. Informat.*, vol. 20, no. 6, pp. 8949–8960, Jun. 2024.
[11] V. Yuvaraju and S. Thangavel, "Optimal phasor measurement unit placement for power system observability using teaching–learning based optimization," *Int. J. Electr. Power Energy Syst.*, vol. 137, May 2022, Art. no. 107775.
[12] J. J. Chavez, N. V. Kumar, S. Azizi, J. L. Guardado, J. Rueda, P. Palensky, V. Terzija, and M. Popov, "PMU-voltage drop based fault locator for transmission backup protection," *Electr. Power Syst. Res.*, vol. 196, Jul. 2021, Art. no. 107188.
[13] B. Mallikarjuna, P. Varma, S. Samir, M. Reddy, and D. Mohanta, "An adaptive supervised wide-area backup protection scheme for transmission lines protection," *Protection Control Mod. Power Syst.*, vol. 2, no. 1, pp. 1–16, Jul. 2017.
[14] A. Sharafi, M. Sanaye-Pasand, and F. Aminifar, "Transmission system wide-area back-up protection using current phasor measurements," *Int. J. Electr. Power Energy Syst.*, vol. 92, pp. 93–103, Nov. 2017.
[15] S. Belagoune, N. Bali, A. Bakdi, B. Baadji, and K. Atif, "Deep learning through LSTM classification and regression for transmission line fault detection, diagnosis and location in large-scale multi-machine power systems," *Measurement*, vol. 177, Jun. 2021, Art. no. 109330.
[16] D. Akmaz, M. S. Mamis, M. Arkan, and M. E. Tagluk, "Transmission line fault location using traveling wave frequencies and extreme learning machine," *Electr. Power Syst. Res.*, vol. 155, pp. 1–7, Feb. 2018.
[17] S. Das, S. P. Singh, and B. K. Panigrahi, "Transmission line fault detection and location using wide area measurements," *Electr. Power Syst. Res.*, vol. 151, pp. 96–105, Oct. 2017.
[18] Z. Jianwen, H. Hui, G. Yu, H. Yongping, G. Shuping, and L. Jianan, "Single-phase ground fault location method for distribution network based on traveling wave time-frequency characteristics," *Electr. Power Syst. Res.*, vol. 186, Sep. 2020, Art. no. 106401.
[19] S. S. Gururajapathy, H. Mokhlis, and H. A. Illias, "Fault location and detection techniques in power distribution systems with distributed generation: A review," *Renew. Sustain. Energy Rev.*, vol. 74, pp. 949–958, Jul. 2017.
[20] M. Korkali, H. Lev-Ari, and A. Abur, "Traveling-wave-based fault-location technique for transmission grids via wide-area synchronized voltage measurements," *IEEE Trans. Power Syst.*, vol. 27, no. 2, pp. 1003–1011, May 2012.
[21] R. A. de Aguiar, A. L. Dalcastagnê, H. H. Zürn, and R. Seara, "Impedance-based fault location methods: Sensitivity analysis and performance improvement," *Electr. Power Syst. Res.*, vol. 155, pp. 236–245, Feb. 2018.
[22] J. Doria-Garcia, C. Orozco-Henao, L. U. Iurinic, and J. D. Pulgarín-Rivera, "High impedance fault location: Generalized extension for ground faults," *Int. J. Electr. Power Energy Syst.*, vol. 114, Jan. 2020, Art. no. 105387.
[23] S. Didehvar and R. Mohammadi Chabanloo, "Accurate estimating remote end equivalent impedance for adaptive one-ended fault location," *Electr. Power Syst. Res.*, vol. 170, pp. 194–204, May 2019.
[24] T. Spielböck and A. Beláň, "Design of a one-sided, impedance-based transmission line fault locator using line topology and source impedances," *Electr. Power Syst. Res.*, vol. 161, pp. 123–138, Aug. 2018.
[25] M. A. Elsadd and A. Y. Abdelaziz, "Unsynchronized fault-location technique for two- and three-terminal transmission lines," *Electr. Power Syst. Res.*, vol. 158, pp. 228–239, May 2018.
[26] M. Ghazizadeh-Ahsaee, "Accurate arcing fault location method for M-terminal transmission lines," *Int. J. Electr. Power Energy Syst.*, vol. 98, pp. 147–155, Jun. 2018.
[27] Y.-J. Lee, T.-C. Lin, and C.-W. Liu, "Multi-terminal nonhomogeneous transmission line fault location utilizing synchronized data," *IEEE Trans. Power Del.*, vol. 34, no. 3, pp. 1030–1038, Jun. 2019.
[28] J. Mora-Florez, J. Meléndez, and G. Carrillo-Caicedo, "Comparison of impedance based fault location methods for power distribution systems," *Electr. Power Syst. Res.*, vol. 78, no. 4, pp. 657–666, Apr. 2008.
[29] J. Hu and A. V. Vasilakos, "Energy big data analytics and security: Challenges and opportunities," *IEEE Trans. Smart Grid*, vol. 7, no. 5, pp. 2423–2436, Sep. 2016.
[30] A. G. Shaik and R. R. V. Pulipaka, "A new wavelet based fault detection, classification and location in transmission lines," *Int. J. Elect. Power Energy Syst.*, vol. 64, pp. 35–40, Jan. 2015.
[31] S. Kanwal and S. Jiriwibhakorn, "Advanced fault detection, classification, and localization in transmission lines: A comparative study of ANFIS, neural networks, and hybrid methods," *IEEE Access*, vol. 12, pp. 49017–49033, 2024.
[32] A. Ramadevi, K. Srilakshmi, P. K. Balachandran, I. Colak, C. Dhanamjayulu, and B. Khan, "Optimal design and performance investigation of artificial neural network controller for solar-and battery-connected unified power quality conditioner," *Int. J. Energy Res.*, vol. 2023, no. 1, 2023, Art. no. 3355124.
[33] K. Khalil, O. Eldash, A. Kumar, and M. Bayoumi, "Machine learning-based approach for hardware faults prediction," *IEEE Trans. Circuits Syst. I, Reg. Papers*, vol. 67, no. 11, pp. 3880–3892, Nov. 2020.
[34] K. Khalil, O. Eldash, A. Kumar, and M. Bayoumi, "Intelligent fault-prediction assisted self-healing for embryonic hardware," *IEEE Trans. Biomed. Circuits Syst.*, vol. 14, no. 4, pp. 852–866, Aug. 2020.
[35] S. Ganesan, P. W. David, P. Murugesan, and P. K. Balachandran, "Solar photovoltaic system performance improvement using a new fault identification technique," *Electr. Power Compon. Syst.*, vol. 52, no. 1, pp. 42–54, Jan. 2024.
[36] S. Ganesan, P. W. David, P. K. Balachandran, and T. Senjyu, "Fault identification scheme for solar photovoltaic array in bridge and honeycomb configuration," *Electr. Eng.*, vol. 105, no. 4, pp. 2443–2460, Aug. 2023.
[37] S. Ekici, "Support vector machines for classification and locating faults on transmission lines," *Appl. Soft Comput.*, vol. 12, no. 6, pp. 1650–1658, Jun. 2012.
[38] Z. Huang, X. Wen, J. Zhu, and Z. Feng, "Research on fault location of DC line in UHV converter station based on digital twin technology," *Meas., Sensors*, vol. 33, Jun. 2024, Art. no. 101180. [Online]. Available: https://www.sciencedirect.com/science/article/pii/S2665917424001569
[39] C. Yang, B. Cai, Q. Wu, C. Wang, W. Ge, Z. Hu, W. Zhu, L. Zhang, and L. Wang, "Digital twin-driven fault diagnosis method for composite faults by combining virtual and real data," *J. Ind. Inf. Integr.*, vol. 33, Jun. 2023, Art. no. 100469.
[40] C. Yang, B. Cai, R. Zhang, Z. Zou, X. Kong, X. Shao, Y. Liu, H. Shao, and J. Akbar Khan, "Cross-validation enhanced digital twin driven fault diagnosis methodology for minor faults of subsea production control system," *Mech. Syst. Signal Process.*, vol. 204, Dec. 2023, Art. no. 110813.
[41] C. C. Ukwuoma, D. Cai, O. Bamisile, E. J. Chukwuebuka, E. Favour, G. S. A. Emmanuel, A. Caroline, and S. F. Abdi, "Power transmission system's fault location, detection, and classification: Pay close attention to transmission nodes," *Int. J. Electr. Power Energy Syst.*, vol. 156, Feb. 2024, Art. no. 109771.
[42] F. Rafique, L. Fu, and R. Mai, "End to end machine learning for fault detection and classification in power transmission lines," *Electr. Power Syst. Res.*, vol. 199, Oct. 2021, Art. no. 107430.
[43] R. V. Rao, V. J. Savsani, and D. P. Vakharia, "Teaching–learning-based optimization: A novel method for constrained mechanical design optimization problems," *Comput.-Aided Des.*, vol. 43, no. 3, pp. 303–315, Mar. 2011.

[44] S. Siva Suriya Narayanan and S. Thangavel, "Machine learning-based model development for battery state of charge–open circuit voltage relationship using regression techniques," *J. Energy Storage*, vol. 49, May 2022, Art. no. 104098.
[45] J. B. P. Matos, E. B. de Lima Filho, I. Bessa, E. Manino, X. Song, and L. C. Cordeiro, "Counterexample guided neural network quantization refinement," *IEEE Trans. Comput.-Aided Design Integr. Circuits Syst.*, vol. 43, no. 4, pp. 1121–1134, Apr. 2024.
[46] M. Jamil, S. K. Sharma, and R. Singh, "Fault detection and classification in electrical power transmission system using artificial neural network," *SpringerPlus*, vol. 4, no. 1, pp. 1–13, Dec. 2015.
[47] K. Vijayaprabakaran and K. Sathiyamurthy, "Towards activation function search for long short-term model network: A differential evolution based approach," *J. King Saud Univ.-Comput. Inf. Sci.*, vol. 34, no. 6, pp. 2637–2650, Jun. 2022.
[48] J. Zhu and W. Zhang, "Application of improved DNN algorithm based on feature fusion in fine-grained image recognition," *IEEE Access*, vol. 12, pp. 32140–32151, 2024.
[49] J. Bae, S.-J. Buu, and S. Lee, "Anchor-net: Distance-based self-supervised learning model for facial beauty prediction," *IEEE Access*, vol. 12, pp. 61375–61387, 2024.
[50] T. Singh, M. Kundroo, and T. Kim, "WSN-driven advances in soil moisture estimation: A machine learning approach," *Electronics*, vol. 13, no. 8, p. 1590, Apr. 2024.
[51] G. Dudek, "Generating random weights and biases in feedforward neural networks with random hidden nodes," *Inf. Sci.*, vol. 481, pp. 33–56, May 2019.
[52] L. Li and J. Hu, "Fast-converging and low-complexity linear massive MIMO detection with L-BFGS method," *IEEE Trans. Veh. Technol.*, vol. 71, no. 10, pp. 10656–10665, Oct. 2022.
[53] D. C. Liu and J. Nocedal, "On the limited memory BFGS method for large scale optimization," *Math. Program.*, vol. 45, nos. 1–3, pp. 503–528, Aug. 1989.
[54] I. A. T. Hashem, F. A. Alaba, M. H. Jumare, A. O. Ibrahim, and A. W. Abulfaraj, "Adaptive stochastic conjugate gradient optimization for backpropagation neural networks," *IEEE Access*, vol. 12, pp. 33757–33768, 2024.

V. YUVARAJU (Graduate Student Member, IEEE) received the B.E. degree in electrical and electronics engineering from the Government College of Engineering, Salem, Tamil Nadu, India, in 2006, and the M.E. degree in power systems engineering from the Government College of Technology, Coimbatore, Tamil Nadu, in 2009. He is currently pursuing the Ph.D. degree with the National Institute of Technology Puducherry, Karaikal, Puducherry, India. He has nine years of teaching experience as an Assistant Professor, from 2010 to 2019, and five years of research experience, since 2019. His research interests include machine learning applications to smart grid protection, artificial intelligence applications to fault detection classification, and localization, and optimal phasor measurement unit placement.

S. THANGAVEL (Senior Member, IEEE) was born in Tamil Nadu, India. He received the B.E. degree in electrical and electronics engineering from the Government College of Technology, Coimbatore, India, in 1993, the M.E. degree in control and instrumentation from the College of Engineering Guindy, Anna University, Chennai, India, in 2002, and the Ph.D. degree in electrical engineering from Anna University, in 2008. He is currently an Associate Professor with the Department of Electrical and Electronics Engineering, National Institute of Technology Puducherry, Karaikal, Puducherry, India. He has published 71 articles in international and national journals, and 21 papers in international and national conferences. His research interests include intelligent controllers, smart grid systems, and industrial drives. He is a fellow in IE(I) and a Life Member in ISTE. He has received four awards which include a national award, best teacher award, best paper award, and outstanding contribution for reviewing.

MALLIKARJUNA GOLLA was born in Nellore, Andhra Pradesh, India. He received the B.Tech. and M.Tech. degrees in electrical and electronics engineering from Jawaharlal Nehru Technological University-Hyderabad (JNTUH), in 2010 and 2014, respectively, and the Ph.D. degree from the National Institute of Technology Puducherry (NITPY), Karaikal, in 2022. From 2013 to 2017, he was an Assistant Professor with the TKR College of Engineering Technology, Hyderabad. Also, he has about five years of research experience as a JRF, SRF, and Postdoctoral Research Associate for DST funded projects at NIT Puducherry and IIT Roorkee. He is currently a Senior Assistant Professor with the School of Electrical Engineering, Vellore Institute of Technology (VIT), Vellore Campus, Tamil Nadu, India. His research interests include grid integration of renewable energy sources, active power filters, artificial neural networks, microgrid, smart grid, and power condition with power flow management.